



1 **Investigating the Local Scale Influence of Sea Ice on 2 Greenland Surface Melt**

3

4 Julianne C. Stroeve^{1,2}, John R. Mioduszewski³, Asa Rennermalm⁴, Linette N. Boisvert⁵ and
5 Marco Tedesco⁶, David Robinson⁴

6 ¹National Snow and Ice Data Center, Cooperative Institute for Research in Environmental
7 Sciences, University of Colorado, 449 UCB, Boulder, CO 80309, USA.

8 ²Centre for Polar Observation and Modelling, University College London, Department of
9 Earth Sciences, Gower Street, London, WC1E6BT, UK.

10 ³Center for Climatic Research, University of Wisconsin – Madison, 1225 W. Dayton St.,
11 Madison, WI 53706, USA.

12 ⁴Department of Geography, Rutgers, The State University of New Jersey, 54 Joyce Kilmer
13 Avenue, Piscataway NJ 08854-8045, USA.

14 ⁵NASA Goddard Space Flight Center, Greenbelt, MD, 20771, USA.

15 ⁶Lamont, Columbia University

16

17 **Abstract**

18 Rapid decline in Arctic sea ice cover in the 21st century may have wide-reaching effects on
19 the Arctic climate system, including the Greenland ice sheet mass balance. Here, we
20 investigate whether local changes in sea ice around the Greenland ice sheet have had an
21 impact on Greenland surface melt. Specifically, we investigate the relationship between sea
22 ice concentration, the timing of melt onset and open water fraction surrounding Greenland
23 with ice sheet surface melt using a combination of remote sensing observations, and
24 outputs from a reanalysis model and a regional climate model for the period 1979 - 2015.
25 Statistical analysis points to covariability between Greenland ice sheet surface melt and sea
26 ice within Baffin Bay and Davis Strait. While some of this covariance can be explained by
27 simultaneous influence of atmospheric circulation anomalies on both the sea ice cover and
28 Greenland melt, within Baffin Bay we find a modest correlation between detrended melt
29 onset over sea ice and the adjacent ice sheet melt onset. This correlation appears to be
30 related to increased transfer of sensible and latent heat fluxes from the ocean to the
31 atmosphere in early sea ice melt years, increasing temperatures and humidity over the ice
32 sheet that in turn initiate ice sheet melt.
33



34 1. Introduction

35 The shrinking sea ice cover is one of the most striking features of Arctic climate change
36 [e.g. Stroeve *et al.*, 2012; Serreze *et al.*, 2007]. Since the late 1970s, the sea ice extent (SIE)
37 has declined by more than 40% in September, with smaller, yet statistically significant
38 negative trends in other months. These negative trends have been linked to the observed
39 increases in atmospheric CO₂, with the prospect of the Arctic Ocean becoming seasonally
40 ice free before the middle of this century if current emission rates continue [Notz and
41 Stroeve, 2016]. At the same time, the Greenland ice sheet (GrIS) has experienced increased
42 summer melt [e.g. Tedesco *et al.*, 2011; Fettweis *et al.*, 2011] and an increasingly negative
43 mass balance [Khan *et al.*, 2015]. While earlier studies found GrIS mass loss to be
44 balanced by ice discharge and ice melt [van den Broeke *et al.*, 2009], newer evidence
45 shows surface melting is now contributing 84% to the mass loss since 2009 [Enderlin *et*
46 *al.*, 2014]. It has further been suggested that surface melting will dominate Greenland's
47 contribution to sea level rise throughout the rest of this century [Enderlin *et al.*, 2014; Fyke
48 *et al.*, 2014]. Similar to the sea ice environment, an anthropogenic signal has been
49 identified in the observed changes of GrIS surface mass balance (SMB) [Fyke *et al.*, 2014].

50 While both the GrIS and sea ice environments are responding to anthropogenic
51 warming [Hanna *et al.*, 2008], changes in atmospheric circulation patterns that favor
52 increased sea ice loss and GrIS melt have also played a role. Analysis of summer (JJA) sea
53 level pressure (SLP) reveal statistically significant increases over Greenland and north of
54 the Canadian Arctic Archipelago coupled with significant negative trends over northern
55 Eurasia and Canada from 1979 to 2014 [Serreze *et al.*, 2016], dominated by a clear shift in
56 the last decade (2005 to 2014) towards large positive SLP anomalies over the central Arctic
57 Ocean and Greenland. This pattern favors both summer sea ice loss [e.g. Wang *et al.*, 2009;
58 Ogi and Wallace, 2007] as well as Greenland surface melt [Hanna *et al.* 2013;
59 Mioduszewski *et al.*, 2016]. Additionally, advection of warm and humid air masses appears
60 to be the primary factor initiating sea ice melt onset [Boisvert and Stroeve, 2015; Mortin *et*
61 *al.*, 2016]. Anomalous GrIS melting also appears to coincide with increasing water vapor
62 transport to the ice sheet [Mattingly *et al.*, 2016]. Thus, it is not surprising that there is a
63 strong inverse correlation between GrIS melt intensity (defined by Tedesco *et al.*, 2007)
64 and the pan-Arctic September SIE ($r = -0.83$ from 1979 to 2015) [Figure 1]. Detrended
65 data reveal a substantially weaker inverse relationship ($r = -0.27$), yet the year-to-year
66 variability between September SIE and GrIS melt remains highly correlated ($r = -0.69$).
67 This would suggest that atmospheric processes fostering a high melt year also tend to foster
68 more summer sea ice loss and vice versa.

69 What about local-scale feedbacks? Changes in sea ice have strong local-scale
70 influences on the Arctic climate through enhanced transfer of heat and moisture between
71 the ocean and atmosphere, resulting in amplified Arctic warming [e.g. Serreze *et al.*, 2009;
72 Screen and Simmonds, 2010]. This is mostly manifested during the cold season, as
73 warming of the ocean mixed layer during summer results in increased sensible and latent
74 heat transfer from the ocean to the atmosphere [Boisvert *et al.*, 2015]. Other studies have
75 linked sea ice loss to atmospheric warming in surrounding areas during other times of the
76 year as well [Comiso *et al.*, 2002; Hanna *et al.*, 2004; Bhatt *et al.*, 2010, Serreze *et al.*,
77 2011]. Sea ice loss is additionally tied to increased tropospheric moisture, precipitation,
78 cloud cover, surface temperature, and decreased static stability [Deser *et al.*, 2000; Rinke *et*
79 *al.*, 2006; Francis *et al.*, 2009; Serreze *et al.*, 2009; Kay *et al.*, 2011; Screen and
80 Simmonds, 2010; Stroeve *et al.*, 2011; Overland and Wang, 2010; Cassano *et al.*, 2014].



81 Water vapor or moisture increases surface melting through its role in cloud formation and
82 as a greenhouse gas, results in increased downward longwave radiation and precipitation
83 [Bennartz *et al.*, 2013, Doyle *et al.*, 2015, van Tricht *et al.*, 2016].

84 This study examines whether or not local changes in the sea ice environment around
85 Greenland are already impacting GrIS meltwater production and therefore SMB variations.
86 First, we identify regions of SIC and GrIS melt covariability by applying the singular value
87 decomposition method. We hypothesize that regions of covariability will have consistent
88 trends in sea ice cover and melt production, as well as consistent trends in spring melt onset
89 and fall freeze up. As a second step, this hypothesis is examined with a spatial analysis of
90 trends for the entire study domain. Third, we investigate if a plausible mechanism for local
91 scale influence between SIC and GrIS is present. Specifically, we hypothesize that the
92 mechanism for the local scale influence is controlled by positive turbulent fluxes from the
93 SIC regions. Therefore, anomalous turbulent fluxes should be larger in years with early sea
94 ice melt onset than in later years in regions of covariability. In turn, these turbulent heat
95 fluxes should result in increased specific humidity and near surface temperature over the
96 GrIS, which should be reflected in positive net longwave radiation anomalies. Finally, a
97 detailed analysis, restricted to the region with evidence of local scale influence, is
98 performed. In this analysis, we examine the hypotheses that the timing of turbulent heat
99 flux anomaly perturbations over reduced sea ice areas proceeds changes in GrIS humidity
100 and temperature, and that wind patterns in early melt onset years are favorable for turbulent
101 heat flux transport from the ocean to the ice sheet. Finally, correlation and partial
102 correlation analysis is used to examine the influence of large scale atmospheric circulation
103 (here represented by the Greenland Blocking Index).

104 2. Data

105 2.1 Sea Ice and Ice Sheet Data

106 Sea ice and Greenland melt extent/area calculations rely on algorithms applied to
107 satellite passive microwave data from the Nimbus-7 Scanning Multichannel Microwave
108 Radiometer (SMMR: 1978-1987) and the DMSP Special Sensor Microwave/Imagers
109 (SSM/I and SSMIS: 1987-present). Specifically, we use several sea ice metrics derived
110 from the NASA Team SIC algorithm [Cavalieri *et al.*, 1996, updated 2008] and distributed
111 by the National Snow and Ice Data Center (NSIDC). The data set spans October 1978 to
112 present, providing daily (or every other day during the SMMR era) SIC estimates. Using
113 the SIC, we additionally calculate the open water fraction (OWF) as well as the length of
114 the ice-free season, defined as the number of days each year with ice concentration less
115 than 15% [see Parkinson, 2014].

116 Changes in the timing of melt onset (MO) and freeze-up (FO), in addition to total melt
117 season length over sea ice, are computed following Markus *et al.* [2009]. This study uses
118 an updated version of the algorithm that bias corrects for intersensor calibration issues
119 found between the F17 and F13 sensor and evaluates early melt onset (EMO),
120 corresponding to the first day of MO, the continuous MO and the continuous FO.

121 GrIS melt extent is an estimate of the daily spatial extent of wet snow using the Mote *et*
122 *al.* [2014] algorithm and distributed by NSIDC. From the binary melt/no melt
123 classification, GrIS MO and FO dates were calculated for each pixel and each year from
124 1979 to 2015. We defined the start of the MO and FO as the first occurrence of a 5-day
125 continuous melt or freeze-up period. Melt duration was calculated as the number of days



126 between MO and FO. EMO was also determined and defined as the first time a spurious
127 melt event lasting at least one day was recorded.

128 Besides mapping the GrIS melt extent and timing of MO and FO, we use meltwater
129 production and 850 hPa wind as simulated by Modèle Atmosphérique Régional (MAR)
130 v3.2 regional climate model [Tedesco *et al.*, 2013]. MAR is a three-dimensional coupled
131 atmosphere-land surface model that uses reanalysis data at its lateral boundaries. In this
132 study, MAR is forced with data from ERA-40 for the period 1979–2002 and ERA-Interim
133 for the period 2002–2015 and outputs are produced on a polar stereographic projection
134 with an approximate grid cell size of 25 x 25 km to match the passive microwave-derived
135 fields. MAR's atmospheric model is coupled to the 1-D Surface Vegetation Atmosphere
136 Transfer scheme, SISVAT [Gallée and Schayes, 1994; De Ridder and Gallée, 1998], which
137 simulates surface properties and the exchange of mass and energy. SISVAT incorporates a
138 snow model based on the CROCUS snowpack model [Brun *et al.*, 1992]. MAR has been
139 validated through comparison with ground measurements [e.g. Lefebvre *et al.*, 2003; Gallée
140 *et al.*, 2005; Lefebvre *et al.*, 2005], satellite data [e.g. Fettweis *et al.*, 2005, 2011; Tedesco *et
141 al.*, 2011, Alexander *et al.*, 2014], and applied to simulate long-term changes in the GrIS
142 SMB and surface melt extent [Fettweis *et al.*, 2005, 2011; Tedesco *et al.*, 2008, 2011;
143 Tedesco and Fettweis, 2012]. Data are freely available from an online repository [Tedesco
144 *et al.*, 2015].

145 Meltwater production was used for grid cells classified by MAR as greater than 99%
146 ice sheet to mask the tundra region of Greenland. In addition, meltwater production values
147 of less than 1 mm day⁻¹ in all grid cells were recoded to zero to account for MAR's scaled
148 output. This threshold could be considered a conservative approximation of the occurrence
149 of surface melt [Fettweis *et al.*, 2011, Figure 2]. Finally, grid cells were masked in the
150 interior ice sheet where mean monthly meltwater production does not exceed 1 mm day⁻¹ to
151 account for spurious correlations arising from a very limited number of dates that result in
152 nonzero mean monthly values of meltwater production.

153 Trends for each pixel (or regional averages) are only computed if at least 30 years of valid
154 data are found at that pixel. This ensures statistics are not biased by changes in spatial extent of
155 the sea ice or Greenland melt. However, Greenland melt has been observed to extend to higher
156 elevations in recent years, and in 2012 nearly the entire ice sheet experienced melt events [e.g.
157 Nghiem *et al.*, 2012]. Regional means are area-weighted. Trends are computed using linear-
158 least squares and statistical significance is evaluated with a student T-test.

159 **2.2 Atmospheric Data**

160 Geopotential heights at 500 hPa and hourly 10 m wind speeds were obtained from
161 NASA's Modern Era Retrospective-Analysis for Research and Applications (MERRA)
162 products [Bosilovich *et al.*, 2011; Cullather and Bosilovich, 2011a, 2011b; Rienecker *et al.*,
163 2011]. MERRA is run on a 1/2° latitude by 2/3° longitude global grid with 72 hybrid-sigma
164 vertical levels to produce analyses from 1979 to present. MERRA has been evaluated
165 extensively since its release [Cullather and Bosilovich, 2011b; Kennedy *et al.*, 2011;
166 Reichle *et al.*, 2011] and has compared favorably with other reanalysis products in the
167 Arctic [Zib *et al.*, 2012; Cullather and Bosilovich, 2011; Lindsay *et al.*, 2014].

168 We also utilize atmospheric variables from NASA's Atmospheric Infrared Sounder
169 (AIRS), designed specifically to map atmospheric water vapor content. This instrument has
170 been used in several recent studies to document atmospheric changes and impacts on sea
171 ice in the Arctic [e.g. Boisvert and Stroeve, 2015; Stroeve *et al.*, 2014; Serreze *et al.*, 2016].
172 While the data record is rather short (begins in September 2002), it provides twice daily



173 global coverage at 1-degree spatial resolution of several key atmospheric variables,
174 including skin and air temperature, precipitable water, cloud fraction and specific humidity.
175 In this study we utilize the Level 3 Version 6 skin temperatures, 1000 hPa air temperature,
176 effective cloud fraction, near surface specific humidity and total precipitable water.
177 Additional variables derived from AIRS data products include the moisture flux [Boisvert
178 *et al.*, 2013; 2015], turbulent sensible heat flux and downwelling longwave radiation
179 [Boisvert *et al.*, 2016].

180 **3. Methods**

181 **3.1. Region of Interest and Study periods**

182 For local assessment of sea ice changes and corresponding ice sheet changes, we define 5
183 sea ice and 5 adjacent ice sheet regions. Since we are examining the potential influence of the
184 ocean on the ice sheet, it makes sense for the ocean regions selected to define the ice sheet
185 boundaries, rather than the other way around. The definition of the sea ice boundaries comes
186 from the International Hydrographic Organization, and we define 5 sea ice regions: Baffin Bay,
187 David Strait, Lincoln Sea, Greenland Sea and the North Atlantic together with associated
188 Greenland regions [Figure 2]. For the ice sheet, each region is defined along a topographical
189 divide. While there are many local topographical divides, only those regions that matched the
190 ocean delineations were selected.

191 We use two study periods. First, we do analysis from 1979 to 2015 when analyzing sea ice,
192 melt extent and MAR model outputs. Second, AIRS data analysis is applied from 2003 to 2015
193 since a full year of data collection didn't begin until 2003.

194 **3.2 Relationship between SIC and GrIS melt**

195 To investigate covariability between summer SIC, GrIS melt water production, and 500
196 hPa geopotential heights, singular value decomposition (SVD) was applied to two fields at
197 a time to produce pairs of coupled spatial patterns that explain their maximum mean
198 squared temporal covariance [Bretherton *et al.*, 1992].

199 The temporal evolution of each pair's corresponding pattern in the two datasets is
200 represented by the pair's associated expansion coefficients (EC), where subscripts GrIS,
201 SIC and 500 denote the EC for ice sheet melt, sea ice concentration, and 500 hPa heights,
202 respectively. These ECs were used to calculate heterogeneous correlation (HC) maps,
203 which show the correlation coefficients between each EC and the opposing data field. SVD
204 has widely been used to investigate coupled modes of variability, including relationships
205 between Arctic sea ice and snow cover [Ghatak *et al.*, 2010], and Arctic sea ice and
206 atmospheric variables [Stroeve *et al.*, 2008].

207 To further investigate how SIC in these regions is related to GrIS melt, SIC for both
208 regions was spatially aggregated, de-trended and correlated with de-trended time series of
209 GrIS meltwater production and the Greenland Blocking Index (GBI), respectively [NOAA,
210 2015]. The GBI is defined as the 500 hPa geopotential height field averaged between 20° –
211 80° W, 60° – 80° N [Fang, 2004; Hanna *et al.*, 2013], and is used as a metric for large-
212 scale atmospheric circulation patterns over Greenland. To remove the influence of the GBI
213 on both SIC and GrIS melt, we performed a partial correlation analysis of SIC in each
214 region and GrIS meltwater production after the trends in GBI were removed [e.g. Cohen *et*
215 *al.*, 2003].



216 3.3 Energy Balance

217 Following *Koenig et al.* [2014], the net heat flux into the atmosphere (F_{net}) emitted
218 from the ocean is defined by:

(1)

$$220 \quad F_{net} = Q_h + Q_e + LW - SW$$

221 where SW is the downward shortwave radiative flux at the surface, LW is the net upward
222 longwave radiation, Q_h is the sensible heat flux, or heat transferred from the surface to the
223 atmosphere by turbulent motion and dry convection, and Q_e is the latent heat flux, or heat
224 extracted from the surface by evaporation. If the sum of the four right-hand side terms is
225 positive, there is a net flow of heat from the surface to the atmosphere and vice versa.

226 Previous studies have looked at the strong seasonality in F_{net} over the Arctic Ocean
227 [e.g. *Serreze et al.*, 2007], with strong downward fluxes in summer and large upward fluxes
228 in January associated with heat gain and loss, respectively, in the subsurface column.
229 Updated trends from NCEP/NCAR reanalysis confirm that F_{net} trends are small in winter
230 (January to April), except in the Barents Sea as a result of reduced sea ice and increased
231 oceanic heat flux [*Ornheim et al.*, 2016] and also within Baffin Bay, again a result of less
232 winter ice cover. Thus, in these two regions there is a transfer of heat from the ocean to the
233 atmosphere during the winter months, which may spread over the sea ice areas and limit
234 winter ice growth. In summer however (May to August), the direction is generally reversed
235 with large heat fluxes from the atmosphere going towards the surface.

236 In this study we focus on how early sea ice retreat, as indicated by early melt onset
237 during the transition from winter to summer, impacts the heat and moisture fluxes over
238 early formed open water areas, and whether or not this is sufficient to impact Greenland
239 melt. Towards this end, we composite the turbulent fluxes in Eq. 2 for low and high sea ice
240 years, specific to each individual region analyzed using the AIRS data, with positive fluxes
241 showing energy transfer from the surface to the atmosphere. We use the criteria of
242 anomalies in melt onset exceeding 1 standard deviation for each region when compositing.
243 All data are detrended by subtracting the linear trend before computing the composites.

244 4. Results

245 We begin with an assessment of the large-scale relationship between SIC and
246 Greenland melt and its spatial covariability (4.1). This is followed by an analysis of
247 changes in the sea ice cover surrounding Greenland, both in terms of SIC and OWF (4.2),
248 followed by analysis of the timing of sea ice MO onset and FO, and its relationship with
249 Greenland MO (4.3). Finally, turbulent heat and moisture flux changes composited for
250 early and late melt onset years are examined (4.4) and large-scale influences are examined
251 in section 4.5.

252 4.1 Relationship between Sea Ice and Greenland Melt

253 The leading SVD mode explains the majority of the mean spatial covariance between
254 monthly GrIS meltwater production and SIC in June and July (62%, 73%, respectively) and
255 less than half (42%) in August. HC maps reveal opposing sign of the correlations between
256 the map pairs [Figure 3: columns 1 and 2; and columns 3 and 4] indicating an
257 anticorrelation, meaning that increased ice sheet melt extent covaries with decreased sea
258 ice area (it is irrelevant in the HC maps which is positive and which is negative).
259 Specifically, the covariability of GrIS meltwater production and SIC, expressed as



260 correlations on an HC map, show that sea ice and ice sheet melt strongly covary in two
261 general regions, namely Baffin Bay/Davis Strait in June, and a large part of Beaufort Sea in
262 June and July [**Figure 3(a), (e) and (i)**]. In June, SIC in both the Baffin Bay/Davis Strait
263 and the Beaufort Sea regions have strong correlations with EC_{GrIS} , $|r| > 0.70$, and GrIS
264 meltwater production is highly correlated with EC_{SIC} for the majority of the unmasked ice
265 sheet surface [**Figure 3b**]. The strong correlation in the Beaufort Sea persists in July but
266 not in Baffin Bay/Davis Strait, and neither exhibits a significant correlation in August
267 [**Figure 3(e) and (i)**]. At the same time, GrIS meltwater production correlations with EC_{SIC}
268 are less expansive over the ice sheet in July and August, particularly in southern Greenland
269 [**Figure 3(f) and (j)**].

270 In the second SVD analysis of 500 hPa geopotential heights and GrIS melt water
271 production, the leading SVD mode explains the majority of mean spatial covariance of the
272 two variables in June and July (79% and 60%, respectively), but less than half in August
273 (37%), which are similar values to the leading SVD mode for GrIS melt and SIC [**Figure**
274 **3(c), (g) and (k)**]. The HC maps show a strong tendency for positive height anomalies
275 centered on the Greenland side of the Arctic, though this area shrinks in July and August
276 [**Figure 3(c), (g) and (k)**]. As before, this spatial pattern covaries with GrIS melt water
277 production over most of the ice sheet in June, but is somewhat more restricted in extent in
278 July and August. While SIC and GrIS melt extent covary regionally, large parts of the same
279 areas of the GrIS melt extent region also covary with 500 hPa geopotential height fields.
280 The similar spatial patterns in GrIS melt covariability with SIC and 500 hPa geopotential
281 height fields suggest that the large-scale circulation may be a dominant explanation for the
282 SIC – GrIS melt covariability. Before this possibility is examined more closely, we analyze
283 trends in SIC and GrIS melt patterns and timing.

284 **4.2 Changes in the Sea Ice Cover around Greenland**

285 The above analysis suggests a local-scale influence from SIC on GrIS melt within
286 Baffin Bay and Davis Strait during June. This region of high SIC-GrIS covariability has
287 experienced a sharp drop in SIC since 1979 [**Figure 4**]. In Baffin Bay and Davis Strait, SIC
288 trends are negative in all seasons, and are particularly large in winter (DJF), spring (MAM)
289 and summer (JJA) [**Figure 4a-d**]. In contrast, SIC trends in the East Greenland Sea are
290 mixed, which may in part explain the lack of covariability within this region. Adjacent to
291 the Greenland's east coast, positive SIC trends occur throughout winter and spring. Further
292 east, reductions in SIC are confined to the area where the Odden used to form (c.f. Figure
293 2). During summer and fall, negative SIC anomalies persist along eastern GrIS, though
294 they remain smaller than on the western side. North in the Lincoln Sea region, there is
295 essentially no change in SIC year-round except for slight negative trends in summer.

296 Negative SIC trends have resulted in longer open water periods surrounding Greenland
297 [**Figure 4e**]. Trends in annual open water days are mostly positive everywhere, the
298 exceptions being the Lincoln Sea, which remains ice-covered year around, and the southern
299 part of Davis Strait towards the Labrador Sea, a region where ice has expanded during
300 recent winters. In some locations within Baffin Bay and the East Greenland Sea the number
301 of open water days has increased by as much as 30 to 40 days per decade, but regionally
302 averaged trends are generally on the order of 2 weeks per decade.

303 The strength of the OWF trends and exact timing of when these trends peak around the
304 GrIS reveal large spatial differences [**Figure 5**]. The largest OWF trends occur in Baffin
305 Bay during week 26 (third week of June), and are on the order of $10\% \text{ dec}^{-1}$, with a
306 secondary peak during week 44 (end of October). Further south in Davis Strait, OWF are



307 positive throughout winter and into July ($\sim 5\% \text{ dec}^{-1}$), reflecting both earlier ice retreat and
308 later winter ice formation, with the largest trends during week 52 ($6\% \text{ dec}^{-1}$). East of
309 Greenland, positive OWF trends are found throughout the year in the Greenland Sea, but
310 are considerably weaker than found in Baffin Bay and Davis Strait. Finally, Lincoln Sea
311 OWF trends are mostly negative (except in June and August), though trends are generally
312 less than $1\% \text{ dec}^{-1}$, and are not statistically significant. For comparison the Arctic Ocean
313 OWF trends are also shown, showing peak OWF trends around week 38 (mid-September),
314 reflecting the timing of the pan-Arctic sea ice minimum.

315 **4.3 Changes in the Melt Season**

316 We next examine if there is a link between the timing of EMO, MO, and FO over sea
317 ice and over GrIS. The link between MO and the timing of ice retreat has already been
318 established, with correlations between the detrended melt onset and detrended ice retreat
319 dates greater than 0.4 [See Figure S10, *Stroeve et al.*, 2016].

320 Climatological regional mean values of EMO, MO, FO show that melt begins earlier
321 and freeze-up happens later over the sea ice than it does on the ice sheet, and can be largely
322 explained by temperature dependencies on elevation [**Table 1**]. In western Greenland, the
323 continuous MO period for sea ice begins about 9 days earlier than on the ice sheet in the
324 Baffin Bay region, and 15 days earlier in the Davis Strait region, whereas ice sheet FO
325 occurs on average in early to mid-September, compared to the end of October (Baffin Bay)
326 to the end of November (Davis Strait) over the adjacent sea ice. Similarly, in the Greenland
327 Sea region, MO begins around 20 days earlier over the sea ice than on the ice sheet and FO
328 happens about a month later. In contrast, the Lincoln Sea region exhibits similar timing in
329 both MO and FO, which may be explained by the fact that this is the smallest region, and
330 also the region furthest north where most melting will only occur at lowest GrIS elevations.
331 Since there is little sea ice in the North Atlantic (e.g. regionally the open water season lasts
332 for 360 days), MO and FO dates are not meaningful, but generally show values similar to
333 as that observed in Davis Strait.

334 EMO, MO and FO trends for SIC and GrIS are of the same sign, indicating an overall
335 lengthening of the melt season over the last 37 years in both environments [**Figure 6**].
336 Baffin Bay experiences the largest trends towards earlier MO and later FO, with regionally
337 averaged trends of -8.3 and $+7.8 \text{ days dec}^{-1}$, respectively, statistically significant at 99%
338 confidence [**Table 2**]. This has led to an increase in the melt season length on the order of
339 16 days per decade. GrIS trends in the same region are typically smaller, especially in
340 regards to the timing of freeze-up ($4.6 \text{ days dec}^{-1}$) and melt season duration ($11.1 \text{ days dec}^{-1}$).
341 In contrast, larger statistically significant trends in both MO and FO are seen over the
342 Davis Strait GrIS region, leading to a lengthening of the melt season that is larger than over
343 the adjacent sea ice ($18.7 \text{ days dec}^{-1}$ compared $11.7 \text{ days dec}^{-1}$).

344 On Greenland's eastern side, similar ice sheet/sea ice MO trends are observed, but sea
345 ice FO trends are smaller, and not statistically significant. The exception is the North
346 Atlantic region, which exhibits large positive FO trends of $8.9 \text{ days dec}^{-1}$, resulting in an
347 overall increase in melt season duration of $16.3 \text{ days dec}^{-1}$. However, given the low
348 frequency of sea ice in this region, caution is warranted when interpreting these trends
349 since ocean dynamics play a large role in the year-to-year variability in these values.
350 Nevertheless, the largest trends in melt season duration over the eastern GrIS are also
351 found in the North Atlantic sector ($22.1 \text{ days dec}^{-1}$), primarily a result of earlier MO. The
352 Greenland Sea GrIS sector also exhibits large trends in melt duration ($14.4 \text{ days dec}^{-1}$), but
353 earlier MO and later FO play a nearly equal role here. Interestingly, the Lincoln Sea GrIS



354 region also displays large trends in melt season duration (12.7 days dec^{-1}), considerably
355 larger than seen over the adjacent sea ice (5.5 days dec^{-1}). While the climatological mean
356 timing of MO and FO is broadly similar over both the sea ice and the GrIS in the Lincoln
357 Sea GrIS region, there has been a trend towards much later freeze-up (6.8 days dec^{-1}).

358 Finally, we examine whether there is synchronicity in the timing of melt onset and
359 freeze-up between the sea ice and the ice sheet. In the Baffin Bay sector, the correlations
360 between the sea ice and ice sheet MO and FO (respectively) exceed 0.6 ; $p=0.001$. High
361 correlations ($r>0.6$) are also seen in the Lincoln Sea sector and for EMO in the Greenland
362 Sea sector ($r=0.6$; $p=0.001$). Correlations are reduced when MO, FO and EMO records are
363 detrended, yet remain significant in the Baffin Bay and Lincoln Sea regions: detrended
364 correlations for sea ice and the ice sheet EMO, FO and melt season duration exceed $r=0.5$,
365 $p=0.001$ in Baffin Bay as well as the Lincoln Sea in regards to the MO, $p=0.002$.
366 Elsewhere, no significant relationship is found.

367 **4.4 Impact of sea ice changes on surface energy fluxes**

368 Next we examine the relationship between early and late MO and variations in
369 atmospheric moisture and heat fluxes using lag-correlation and composites for early and
370 late MO years. We begin with an assessment of the differences in the strength of turbulent
371 fluxes between early and late MO years. All months are shown to allow for both an
372 assessment of what drives early MO over sea ice as well as to determine how early sea ice
373 MO influences the overlying atmosphere [Figure 7].

374 On average, the transfer of latent heat flux occurs from the ocean to the atmosphere
375 year-round in all regions, except the Lincoln Sea in Sep-May, and Baffin Bay in Dec-Feb.
376 In Baffin Bay and Lincoln Sea, latent heat flux transferred to the atmosphere is small until
377 the sea ice begins to break up and melt in the summer and moisture is released from the
378 previously ice-covered ocean. Latent heat fluxes are directed into the atmosphere year-
379 round in Davis Strait and Greenland Sea due to large areas of ice-free ocean that persists
380 throughout the year.

381 Sensible heat flux is generally directed towards the surface for regions that are 100%
382 sea ice covered during the cold season months (e.g. Baffin Bay and the Lincoln Sea) and
383 then switches towards the atmosphere as the sea ice retreats in summer (Baffin Bay only).
384 Regions that have large fractions of open water year-round generally have a net sensible
385 heat flux transfer towards the atmosphere year-round, though some exceptions occur.
386 Greenland Sea and Davis Strait exhibit sensible heat flux to the atmosphere in early spring
387 and late fall (October-December) when the ice-free ocean surface is much warmer than the
388 overlying air; due to the higher heat capacity of water, the opposite is true for ice-covered
389 regions.

390 A larger amount of sensible and latent heat flux tends to enter the atmosphere in the
391 spring during early MO years in all regions. However, the Baffin Bay region is the only
392 region with a majority of positive fluxes throughout the year. When melt happens early in
393 Baffin Bay, the additional sensible and latent heat fluxes result in $\sim 14 \text{ Wm}^{-2}$ entering the
394 atmosphere in spring (March-June) and $\sim 25 \text{ Wm}^{-2}$ in autumn (September-December) due
395 to a later FO. In contrast to Baffin Bay, turbulent flux anomalies in early MO years from
396 Davis Strait and Lincoln Sea show no strong consistent pattern and switch between positive
397 anomalies throughout the year. Compared to Baffin Bay, Davis Strait, which is further
398 south, has larger latent heat fluxes entering the atmosphere between February-August
399 during years with earlier MO, whereas sensible heat flux into the atmosphere is only larger
400 during early MO years in February, April and November, reflecting both early MO (April)



401 and later FO (November). Over the Lincoln Sea there are no fluxes of heat or moisture into
402 the atmosphere during the late fall, winter and early spring due to the solid sea ice pack.
403 However, by June there is an additional $\sim 12 \text{ W m}^{-2}$ of turbulent flux energy transferred to
404 the atmosphere during early melt years. This generates smaller turbulent fluxes in July due
405 to warmer air temperatures than when melting has just begun in late MO years. The early
406 MO year turbulent flux anomalies from Greenland Sea are different from the other three
407 regions, as there is more heat and moisture entering the atmosphere in January, March,
408 October and December during early MO years.

409 Sensible and latent heat fluxes transfer heat and moisture into the local atmosphere and
410 can cause the temperature and humidity to increase, which in turn should produce larger
411 downwelling longwave flux at the surface due to the greenhouse feedback effect. Thus one
412 would expect to see a larger net longwave flux (downwelling – upwelling) at the surface
413 during early MO years when the local atmosphere contains more heat and moisture. We see
414 evidence of this occurring until roughly July as there is more net longwave directed
415 towards the surface of the ice sheet in most regions when the sea ice melts earlier [Figure
416 8]. In August the surface net longwave flux turns largely negative during early MO years,
417 partly because the warmer ice sheet results in dominance of upwelling radiation fluxes, and
418 partly because there is less of an influence of early season conditions.

419 The increase in heat and moisture into the atmosphere from the surrounding ocean in
420 early MO versus late MO years and subsequent increase in energy at the ice sheet surface is
421 shown in more detail for Baffin Bay in **Figures 9(a) and (b)**. In April and May (day 1 to 61
422 in Figure 9), there appears to be an out-of-phase relationship between latent heat flux over
423 Baffin Bay and the specific humidity over the adjacent ice sheet, with pulses of moisture
424 coming from the ocean surface being followed about a week later with rising specific
425 humidity over the ice sheet. A similar pattern is observed between ocean sensible heat flux
426 and near surface air temperature over GrIS. In June and July (day 61 to 92), latent and
427 sensible heat flux anomalies for early/late MO years fluctuate around zero, which suggests
428 these fluxes are similar between early and late MO years. In contrast, the specific humidity
429 and temperature are higher in late MO years over the ice sheet in July (negative anomalies
430 in Figure 9a and 9b). This could be due to a roughly one-month delay in late MO years
431 compared to early MO for the sea ice, which causes increases in the temperatures and
432 humidity later in the season (July) over the ice sheet. From the timing of early sea ice MO
433 (dotted blue line) to early GrIS MO (dotted blue, highlighted red line), large fluxes of
434 moisture and heat released via the latent and sensible heat flux from the ice/ocean surface
435 precede elevated humidity and temperature over the ice sheet.

436 One-week running lagged correlations between latent heat flux from the ocean and
437 specific humidity over the ice sheet show large positive correlations during early MO years
438 [Figure 9a top, solid blue lines], suggesting increased evaporation from earlier MO over
439 sea ice may be driving the observed increase in specific humidity over the ice sheet one
440 week later. A one-week lag was chosen because sea ice and GrIS MO in Baffin Bay occur
441 about 9 days apart on average, and also because water vapor in the troposphere has a
442 residence time of about two weeks. These three highly correlated events precondition the
443 ice sheet for earlier MO by increasing the specific humidity and thus the downwelling
444 longwave flux earlier in the spring. In late MO years, the sea ice/ocean does also appear to
445 play a small role in initiating MO on the ice sheet. Large amounts of latent heat are
446 released from the surface in Baffin Bay at the timing of late MO, which in turn is correlated
447 to increases in specific humidity over the ice sheet directly before MO, initiating melt
448 (solid green lines). Since Baffin Bay MO is much later (~ 1 month) in late melt years,



449 excess moisture into the atmosphere is delayed. Though because the environment is already
450 warming seasonally, it does not require extra preconditioning for the melt to begin on GrIS
451 compared to early melt years. This case is very similar to sensible heat flux released from
452 Baffin Bay and ensuing temperature over the ice sheet [**Figure 9b**]. Comparing these 1-
453 week lagged correlations to a zero-lag correlation (not shown), correlations for all variables
454 in early and late MO years are highly negative, meaning they are out of phase.

455 Note also there are instances in April when both early and late melt years exhibit high
456 correlations between either sensible or latent heat from the sea ice region and specific
457 humidity or temperature over GrIS one week later. This may be related to opening of the
458 North Water Polynya [Boisvert *et al.*, 2012]. As the open ocean is relatively warm
459 compared to the overlying air in April, heat and moisture fluxes enter the atmosphere and
460 are subsequently transferred over the ice sheet, increasing the specific humidity and air
461 temperature.

462 In summary, sea ice in Baffin Bay/Davis Strait and the adjacent ice sheet surface
463 conditions appear connected. MO and breakup of the sea ice triggers enhanced flux of heat
464 and moisture into the atmosphere, which are observed over the ice sheet within a week.
465 This results in a warming and moistening the local environment and preconditions the ice
466 sheet for melt in early MO years. Therefore, when the MO of the sea ice is earlier, MO of
467 GrIS is earlier and vice versa.

468 **4.5 Influence of large scale atmospheric variability on Baffin Bay 469 and Beaufort Sea**

470 The SVD analysis (4.1) indicated that both Baffin Bay/Davis Strait and the Beaufort
471 Sea are regions with SIC and GrIS melt water production covariability. In the case of
472 Baffin Bay/Davis Strait, this was supported by the melt and turbulent heat flux analysis.
473 Next we examine the influence of the large-scale atmospheric variability on this
474 covariability using Pearson correlation and partial correlation.

475 In the Beaufort Sea, both 500 hPa heights and SIC closely covary, particularly in June
476 [**Figure 10a**], in concert with high SIC covariance in this region with EC_{GrIS} in the HC
477 maps [**Figure 3**]. Here, the positive correlations between SIC and GrIS melt weaken
478 significantly after June with almost no correlation by August [**Table 3**]. The strong
479 relationship between Beaufort SIC and GrIS melt in June is reduced considerably when the
480 GBI index is removed via partial correlation, as significant correlations remain only in
481 southeast Greenland.

482 The correlation between SIC in Baffin Bay/Davis Strait and geopotential heights is
483 relatively strong but not as extensive in June, while this signal mostly disappears in July
484 and especially August [**Figure 10d; Table 3**]. This is associated with a weakening Baffin
485 Bay SIC correlation with EC_{GrIS} in the HC maps [**Figure 3(a), (e) and (i)**]. Statistically
486 significant correlations with meltwater production are focused on the west side of the ice
487 sheet in June [**Figure 10e**], but are minimal in July and August when correlations over only
488 7% and 2% of the respective unmasked ice sheet area are statistically significant. Partial
489 correlation analysis indicates that the GBI explains approximately two thirds of this
490 correlation in each month, though this still leaves the possibility that variations in Baffin
491 Bay sea ice are in part responsible for the correlation with surface melt in western
492 Greenland.

493 Because there is a potential local influence from Baffin Bay and Davis Strait, we next
494 focus on GrIS melt only in west-central Greenland. The highest and lowest melt years in



495 west-central Greenland (after removing trends) consistently correspond to patterns of
496 anomalous SIC and geopotential heights in these years [Figure 11]. These variables show
497 much less variation by month, though a weaker relationship appears particularly in the
498 height field, which follows results from the SVD analysis [Figure 11 (g)-(h)]. Additionally,
499 a strong SIC pattern is evident not just in western Greenland but consistently on the east
500 side of Greenland that is equally as strong [Figure 11(a)-(f)]. This suggests that the
501 processes responsible for this signal expression to the west of Greenland probably also
502 exist on a large enough scale to have an effect of similar strength on sea ice off
503 Greenland's east coast; most likely a persistent ridge or trough, as suggested by the above
504 results. By August, sea ice in Baffin Bay has melted in most years, but positive anomalies
505 in SIC still appear in the lowest Greenland melt years [Figure 11(f)].

506 In summary, the SVD analysis suggest covariability between SIC and GrIS melt in the
507 Baffin Bay region (Fig. 3) that cannot fully be explained by large scale atmospheric
508 patterns (Fig 10 and 11). Examination of a set of hypotheses applied for the entire GrIS and
509 surrounding seas shows that trends and patterns in the Baffin and Davis Strait regions are
510 consistent with local scale influence [Table 4]. In contrast, no other regions have evidence
511 of covariability or trends and patterns consistent with local scale influence.

512 5. Discussion

513 Sea ice and Greenland ice sheet melt demonstrate significant covariability during the
514 summer, particularly June. While the majority of this relationship appears related to
515 simultaneous atmospheric circulation forcing, analysis over Baffin Bay/Davis Strait and the
516 adjacent ice sheet indicates that the covariability may additionally include a local-scale
517 influence. This is in agreement with previous work by *Rennermalm et al.* [2009] who found
518 the SIE and GrIS surface melt extent to co-vary in the western part of the ice sheet, though
519 the strongest relationships were found in August rather than June. Part of the discrepancy
520 might be explained by the study period. This study extends through 2015 and includes
521 years with larger anomalies in both SIC and GrIS melt. However, June is the time of year
522 with the largest trends in OWF, reflecting earlier development of open water at a time
523 when the atmosphere is still relatively cold. Thus, it is not surprising that we find stronger
524 covariability in June and a link with melt onset. An additional area of covariability in terms
525 of melt onset timing is also seen in the Lincoln Sea sector.

526 While statistical analysis suggests a local-scale influence may be present on the western
527 side of the ice sheet, the ability for the sea ice to influence GrIS melt depends on having
528 anomalous heat and moisture sources that can travel to the ice sheet. In this study we find
529 that turbulent fluxes are often larger during early MO years in the spring and fall because
530 areas where the ocean is ice-free tends to be warmer than that of the air, due to the higher
531 heat capacity of water. Both latent and sensible heat fluxes are larger and more positive
532 (from the ocean surface to the atmosphere) during early MO years, resulting in increased
533 air temperature and specific humidity especially in May when the atmosphere is ~ 2 K
534 warmer and ~ 0.5 g kg $^{-1}$ wetter. This excess heat and humidity increases downwelling
535 fluxes to the ice sheet earlier in the year, preconditioning the ice sheet and triggering melt
536 (also shown in Figure 8). For late MO years, this phenomena occurs later in the season, and
537 this is most likely why we see larger fluxes during late MO years in the summer months
538 (i.e. July depending on the climatology of the region). This is specifically true for Baffin
539 Bay, where throughout the winter months the region is completely covered by sea ice,
540 creating a barrier between ocean-atmosphere energy exchanges. This is also valid for the



541 Lincoln Sea in the content of melt ponds and a higher occurrence of leads forming on the
542 thick multi-year ice during the summer months.

543 Turbulent fluxes from increased open water can reach well above the boundary layer
544 [e.g. *Yulaeva et al.*, 2001], but this depends on the frequency of spring and early summer
545 inversions that cap the atmospheric boundary layer. Furthermore, if katabatic winds are
546 persistent at the ice edge, this will keep onshore flow from reaching the ice sheet [*Noël et*
547 *al.*, 2014], though a possibility remains for mixing in the boundary layer via a barrier wind
548 mechanism [*van den Broeke and Gallée*, 1996]. Analysis of daily winds around the timing
549 of sea ice melt, show that during early MO years over the sea ice, wind direction is from
550 the open water areas of Baffin Bay onto the GrIS, which helps support our claims that
551 earlier melt onset in part drives early melt over Greenland [**Figure 12**]. In late MO years,
552 the wind direction is reversed.

553 Finally, we note that SVD analysis reveals the strongest relationship between GrIS melt
554 and sea ice variability occurs within the Beaufort Sea. This appears to be related to the
555 positioning of a ridge near Greenland that enhances both ice sheet melt and sea ice retreat
556 as stronger easterlies help to circulate ice west out of the Beaufort Sea. SVD analysis
557 shows the covariability in June is reduced considerably when the GBI index is removed via
558 partial correlation, evidenced by the large reduction in percentage of grid cells with a
559 significant correlation (not shown). This mechanism has been identified previously as a
560 way to transport and melt ice between the Beaufort Sea and the East Siberian Sea [*Rogers*,
561 *1978*; *Maslanik et al.*, 1999]. We speculate that no mechanism originating from sea ice
562 variability directly influences GrIS melt from a distance of hundreds of kilometers away,
563 though Liu et al. (2016) argue that sea ice loss within the central Arctic has favored
564 stronger and more frequent blocking events over Greenland.

565 In 2012, as the sea ice cover reached its all-time record low September extent, the
566 Greenland ice sheet also experienced a record amount of surface melt and ice mass loss
567 [*Tedesco et al.*, 2013]. Several explanations have been put forth to explain this anomalous
568 melt, including increased downwelling longwave radiation from low-level liquid clouds
569 [*Bennartz et al.*, 2013], advection of moist warm air over Greenland [*Neff et al.*, 2014] and
570 dominance of non-radiative fluxes [*Fausto et al.*, 2016]. While this event was likely a result
571 of atmospheric circulation patterns that transported warm, humid air over the southern and
572 western part of the ice sheet, the sea ice melt season began a week earlier than the 1981-
573 2010 long-term mean over Davis Strait and 3 days earlier over Baffin Bay. This earlier
574 melt onset of the sea ice may have provided an additional source of warm, moist air over
575 the adjacent ice sheet.

576 **6. Conclusions**

577 Based on multiple lines of statistical evidence, we identified western Greenland as a
578 region where direct influence from sea ice on the GrIS SMB is possible. SVD analysis
579 revealed that extreme melt years over the adjacent ice sheet are accompanied by strong SIC
580 anomalies within Baffin Bay and Davis Strait that would be expected if a local-scale
581 thermodynamic influence were occurring. This is true even after near surface temperature
582 and climate index influences are removed.

583 The covariance is strongest in June, which may be partially due to the lower variability
584 in interannual June meltwater production over the entire ice sheet relative to the rest of
585 summer, with a standard deviation simulated by MAR of 0.84 mm water equivalent day⁻¹
586 compared to 0.95 in August and 1.12 in July. Additionally, June variability in sea ice may



587 have a greater potential to influence GrIS melt given that the ice sheet is transitioning into
588 its warm season regime and reaching the freezing point for the first time in many locations.
589 This is further confirmed through correlations between the timing of melt onset, which
590 occurs on average 9 days earlier over the sea ice than on the adjacent ice sheet, and in turn
591 allows for earlier development of open water and enhanced transfer of turbulent heat fluxes
592 from the ocean to the atmosphere. More heat and moisture is transported to the local
593 atmosphere from the ice-free ocean surface via turbulent fluxes in years when sea ice melts
594 earlier. Daily wind field analysis suggests these enhanced turbulent fluxes are transferred to
595 the ice sheet, allowing the local atmosphere over the GrIS to warm and become more
596 humid, which in turn impacts the net downwelling longwave flux, helping precondition the
597 surface for earlier melt onset.

598 However, despite evidence of a possible local-scale influence, all analysis incorporating
599 500 hPa height anomalies suggests that the large-scale atmospheric circulation remains the
600 primary melt driver in this part of the ice sheet as well as for the ice sheet as a whole.
601 Anomalous atmospheric circulation features include increased frequency of the negative
602 phase of the Arctic Dipole [Overland and Wang, 2010] and a persistently negative summer
603 North Atlantic Oscillation [van Angelen et al., 2013]. Continued Arctic amplification and
604 associated shifts in Arctic atmospheric circulation and their persistence will theoretically
605 continue to enhance warming in the vicinity of Greenland [Francis and Vavrus, 2012,
606 2015]. Nevertheless, our study suggests a local response is also possible, and as the sea ice
607 cover continues to retreat around the Greenland ice sheet, this should present further
608 opportunities for local enhancement of summer ice sheet melt.

609

610 Acknowledgements

611 This work was funded by the National Science Foundation PLR 1304807. All data used in
612 this study were obtained from free and open data repositories. Detailed information is
613 provided in the methods section. The work of Linette Boisvert was funded from NASA
614 ROSES 2012 IDS proposal: 12-IDS12-0120. AIRS data are freely available at
615 www.airs.jpl.nasa.gov and MERRA2 data can be found at gmao.gsfc.nasa.gov.

616

617 References

618 Alexander, P. M., M. Tedesco, Z. Fettweis, R.S.W. van de Wal, C.J.P.P. Smeets and M.R.
619 van den Broeke (2014), *The Cryosphere*, 8, 2293-2312, doi:10.5194/tc-8-2293-2014.
620 Bennartz, R., M.D. Shupe, D.D. Turner, V.P. Walden, K. Steffen, C.J. Cox, M.S. Kullie,
621 N.B. Miller and C. Pettersen (2013), July 2012 Greenland melt extent enhanced by low-
622 level liquid clouds. *Nature*, **496**, 83–86, doi:10.1038/nature12002.
623 <http://www.nature.com/doifinder/10.1038/nature12002> (Accessed April 3, 2013).
624 Bhatt, U., D.A. Walker, M.K. Reynolds, J.C. Comiso, H.E. Epstein, G. Jia, R. Gens, J.E.
625 Pinzon, C.J. Tucker, C.E. Tweedie, and P.J. Webber (2010), Circumpolar Arctic tundra
626 vegetation change is linked to sea ice decline, *Earth Interactions*,
627 doi:10.1175/2010E1315.1.
628 Boisvert, L. N., A. A. Petty, and J. C. Stroeve (2016), The impact of the extreme winter
629 2015/2016 Arctic cyclone on the Barents-Kara seas, *Monthly Weather Review*,
630 doi:10.1175/WMR-D-16-0234.
631 Boisvert, L. N., D. L. Wu, and C.-L. Shie (2015), Increasing evaporation amounts seen in
632 the Arctic between 2003-2013 from AIRS data, *J. Geophys. Res. Atmos.*, 120, 6865-
633 6881, doi:10.1002/2015JD023258.
634 Boisvert, L.N. and J.C. Stroeve, (2015), The Arctic is becoming warmer and wetter as



635 revealed by the Atmospheric Infrared Sounder, *Geophys. Res. Lett.*,
636 doi:10.1002/2015GL063775.

637 Boisvert, L. N., T. Markus, C. L. Parkinson, and T. Vihma (2012), Moisture fluxes derived
638 from EOS Aqua satellite data for the North Water polynya over 2003-2009, *J. Geophys.*
639 *Res.*, 117, D06119, doi:10.1029/2011JD016949.

640 Bosilovich, M. G., F. R. Robertson, and J. Chen (2011), Global Energy and Water Budgets
641 in MERRA, *J. Clim.*, 24(22), 5721–5739, doi:10.1175/2011JCLI4175.1.

642 Bretherton, C.S, C. Smith and J.M. Wallace (1992), An intercomparison of methods for
643 finding coupled patterns in climate data, *J. Climate*, 5, 451–560.

644 Brun, E., David, P., Sudul, M., and G. Brunot (1992), A numerical model to simulate
645 snow-cover stratigraphy for operational avalanche forecasting. *J. Glaciol.*, 38(128), 13–
646 22.

647 Cassano, E. N., J. J. Cassano, M. E. Higgins, and M. C. Serreze (2014), Atmospheric
648 impacts of an Arctic sea ice minimum as seen in the Community Atmosphere Model,
649 *Int. J. Climatol.*, 34(3), 766–779, doi:10.1002/joc.3723.

650 Cavalieri, D., C. Parkinson, P. Gloersen, and H. J. Zwally (1996), updated 2008. Sea Ice
651 Concentrations from Nimbus-7 SMMR and DMSP SSM/I Passive Microwave Data,
652 [1979-2013]. Boulder, Colorado USA: National Snow and Ice Data Center. Digital
653 media.

654 Cohen, J., P. Cohen, S. G. West, and L. S. Aiken (2003). *Applied multiple*
655 *regression/correlation analysis for the behavioral sciences* (3rd ed.). Routledge,
656 Mahwah.

657 Comiso, J.C., (2002), Correlation and trend studies of the sea-ice cover and surface
658 temperatures in the Arctic, *Annals of Glaciology*, 34(1), pp.420–428.

659 Cullather, R. I., and M. G. Bosilovich (2011a), The Energy Budget of the Polar
660 Atmosphere in MERRA, *J. Clim.*, 25(1), 5–24, doi:10.1175/2011JCLI4138.1.

661 Cullather, R. I., and M. G. Bosilovich (2011b), The Moisture Budget of the Polar
662 Atmosphere in MERRA, *J. Clim.*, 24(11), 2861–2879, doi:10.1175/2010JCLI4090.1.

663 Dee, D.P. and S. Uppala (2009), Variational bias correlation of satellite radiance data in the
664 ERA-Interim reanalysis, *Q. J. R. Meteorol.*, Soc., 135, 1830,1841, doi:10.1002/qj.493.

665 De Ridder, K., and H. Gallée (1998), Land surface-induced regional climate change in
666 southern Israel. *J. Appl. Meteorol.*, 37(11), 1470–1485.

667 Deser, C., J. E. Walsh, and M. S. Timlin (2000), Arctic Sea Ice Variability in the Context
668 of Recent Atmospheric Circulation Trends, *J. Clim.*, 13, 617–633.

669 Doyle, S. H., and Coauthors, (2015), Amplified melt and flow of the Greenland ice sheet
670 driven by late-summer cyclonic rainfall. *Nat. Geosci.*, 8, 647–653,
671 doi:10.1038/ngeo2482. <http://www.nature.com/doifinder/10.1038/ngeo2482>.

672 Enderlin, E.M., I.M. Howat, S. Jeong, M.-J. Noh, J.H. van Angelen and M.R. van den
673 Broeke (2014), An improved mass budget for the Greenland ice sheet, *Geophys. Res.*
674 *Lett.*, 41, doi:10.1002/2013GL059010.

675 Fang Z-F (2004), Statistical relationship between the northern hemisphere sea ice and
676 atmospheric circulation during wintertime. In: *Observation, Theory and Modeling of*
677 *Atmospheric Variability*. World Scientific Series on Meteorology of East Asia, Zhu X
678 (ed), World Scientific.

679 Fausto, R.S., D. van As, J.E. Box, I. Colgan, P.L. Langen and R.H. Mottram, (2016), The
680 implication of nonradiative fluxes dominating Greenland ice sheet exceptional ablation
681 area surface melt in 2012, *Geophys. Res. Lett.*, 43, doi:10.1002/2016GL067720.

682 Fettweis, X., Gallée, H., Lefebvre, F., and J.-P. van Ypersele, (2005), Greenland surface



683 mass balance simulated by a regional climate model and comparison with satellite-
684 derived data in 1990-1991. *Clim. Dyn.*, 24(6), 623-640. doi:10.1007/s00382-005-0010-
685 y.

686 Fettweis, X., M. Tedesco, M. van den Broeke, and J. Ettema (2011), Melting trends over
687 the Greenland ice sheet (1958–2009) from spaceborne microwave data and regional
688 climate models, *The Cryosphere*, 5(2), 359–375, doi:10.5194/tc-5-359-2011.

689 Francis, J.A. and S.J. Vavrus (2012), Evidence linking Arctic amplification to extreme
690 weather in mid-latitudes, *Geophys. Res. Lett.*, 39(6), doi:10.1029/2012GL051000.

691 Francis, J. A., W. Chan, D. J. Leathers, J. R. Miller, and D. E. Veron (2009), Winter
692 Northern Hemisphere weather patterns remember summer Arctic sea-ice extent,
693 *Geophys. Res. Lett.*, 36(7), L07503, doi:10.1029/2009GL037274.

694 Fyke, J.G., M. Vizcaino, W. Lipscomb and S. Price (2014), Future climate warming
695 increases Greenland ice sheet surface mass balance variability, *Geophys. Res. Lett.*, 41,
696 doi:10.1002/2013GL058172.

697 Gallée, H., and G. Schayes (1994), Development of a three-dimensional meso- γ primitive
698 equation model – katabatic winds simulation in the area of Terra-Nova Bay, Antarctica.
699 *Mon. Wea. Rev.*, 122(4), 671-685.

700 Gallée H., Peyaud V., and I. Goodwin (2005), Simulation of the net snow accumulation
701 along the Wilkes Land transect, Antarctica, with a regional climate model. *Ann.*
702 *Glaciol.*, 41, 17-22.

703 Ghatak, D., A. Frei, G. Gong, J. Stroeve, and D. Robinson, (2010). On the emergence of an
704 Arctic amplification signal in terrestrial Arctic snow extent, *J. Geophys. Res.*, 115,
705 D24105, doi:10.1029/2010JD014007.

706 Hanna, E., X. Fettweis, S.H. Mernild, J. Cappelen, M.H. Ribergaard, C.A. Shuman, K.
707 Steffen, L. wood and T.L. Mote (2013), Atmospheric and oceanic climate forcing of the
708 exceptional Greenland ice sheet surface melt in summer 2012. *Int. J. Climatol.*,
709 doi:10.1002/joc.3743.

710 Hanna, E., et al. (2008), Increased runoff from melt from the Greenland ice sheet: A
711 response to global warming, *J. Clim.*, 21, 331 – 341, doi:10.1175/2007JCLI1964.1.

712 Hanna, E., T. Jonsson and J.E. Box, (2004), An analysis of Icelandic climate since the
713 nineteenth Century, *Int. J. Clim.*, 24, doi:10.1002/joc.1051.

714 Kahn, S.A., A. Aschwanden, A.A. Wahr, K.K. Kjeldsen and K.H. Kjaer, (2015), Greenland
715 ice sheet mass balance: a review, *Rep. Prog. Phys.* 78, 046801, 26pp.

716 Kay, J. E., K. Raeder, A. Gettelman, and J. Anderson (2011), The Boundary Layer
717 Response to Recent Arctic Sea Ice Loss and Implications for High-Latitude Climate
718 Feedbacks, *J. Clim.*, 24(2), 428–447, doi:10.1175/2010JCLI3651.1.

719 Lefebvre, F., Gallée, H., van Ypersele, J.P., and W. Greuell (2003), Modeling of snow and
720 ice melt at ETH-Camp (West Greenland): A study of surface albedo. *J. Geophys. Res.*,
721 108(D8), 4231. doi:10.1029/2001JD001160.

722 Lefebvre, F., Fettweis, X., Galée, H., van Ypersele, J.-P., Marbaix, P., Greuell, W., and P.
723 Calanca, (2005), Evaluation of a high-resolution regional climate simulation over
724 Greenland. *Clim. Dyn.*, 25(1), 99-116. doi:10.1007/s00382-005-0005-8.

725 Lindsay, R., M. Wensnahan, a. Schweiger, and J. Zhang (2014), Evaluation of Seven
726 Different Atmospheric Reanalysis Products in the Arctic*, *J. Clim.*, 27(7), 2588–2606,
727 doi:10.1175/JCLI-D-13-00014.1.

728 Liu, J., Z. Chen, J. Francis, M. Song, T. Mote, and Y. Hu (2016), Has Arctic Sea Ice Loss
729 Contributed to Increased Surface Melting of the Greenland Ice Sheet?, *J. Clim.*, 29(9),
730 3373–3386, doi:10.1175/JCLI-D-15-0391.1.



731 Markus, T., J.C. Stroeve and J. Miller (2009), Recent changes in Arctic sea ice melt onset,
732 freezeup and melt season length, *J. Geophys. Res.*, 114, C12024,
733 doi:10.1029/2009JC005436.

734 Mattingly, K. S., C. A. Ramseyer, J. J. Rosen, T. L. Mote, and R. Muthyalu (2016),
735 Increasing water vapor transport to the Greenland Ice Sheet revealed using self-
736 organizing maps, *Geophys. Res. Lett.*, (August), doi:10.1002/2016GL070424.

737 Mioduszewski, J. R., A. K. Rennermalm, A. Hammann, M. Tedesco, E. U. Noble, J. C.
738 Stroeve, and T. L. Mote (2016), Atmospheric drivers of Greenland surface melt revealed
739 by self-organizing maps, *J. Geophys. Res. - Atmos.*, 121, 5095–5114,
740 doi:10.1002/2015JD024550.

741 Mortin, J., G. Svensson, R. Graverson, M-L. Kapsch, J.C. Stroeve and L.N. Boisvert
742 (2016), Melt onset over Arctic sea ice controlled by atmospheric moisture transport,
743 *Geophys. Res. Lett.*, 43(12), doi:10.1002/2016GL069330.

744 Mote, Thomas L. 2014. *MEaSUREs Greenland Surface Melt Daily 25km EASE-Grid 2.0*,
745 [indicate subset used]. Boulder, Colorado USA: NASA DAAC at the National Snow
746 and Ice Data Center. doi: <http://dx.doi.org/10.5067/MEASURES/CRYOSPHERE/nsidc-0533.001>

747 Mote, Thomas L. 2007. Greenland surface melt trends 1973-2007: Evidence of a large
748 increase in 2007. *Geophys. Res. Lett.*, 34, L22507. doi:
749 <http://dx.doi.org/10.1029/2007GL031976>.

750 Neff, W., G. Compo, F.M. Ralph and M.D. Shupe (2014), Continental heat anomalies and
751 the extreme melting of the Greenland ice surface in 2012 and 1889, *J. Geophys. Res.-*
752 *Atmos.*, doi:10.1002/2014JD021470.

753 Noël, B., X. Fettweis, W. J. van de Berg, M. R. van den Broeke, and M. Erpicum, 2014:
754 Sensitivity of Greenland Ice Sheet surface mass balance to perturbations in sea surface
755 temperature and sea ice cover: a study with the regional climate model MAR. *Cryosph.*,
756 8, 1871–1883, doi:10.5194/tc-8-1871-2014.

757 Notz, D. and J. Stroeve (2016), Observed Arctic sea-ice loss directly follows anthropogenic
758 CO₂ emission, *Science*, doi:10.1126/science.aag2345.

759 Ornaheim, I.H., T. Eldevik, M. Arthun, R.B. Ingvaldsen and L.H. Smedsrød (2016),
760 Skillful prediction of Barents Sea ice cover, *Geophys. Res. Lett.*, 42,
761 doi:10.1002/2015GL064359.

762 Overland, J. E., and M. Wang (2010), Large-scale atmospheric circulation changes are
763 associated with the recent loss of Arctic sea ice, *Tellus A*, 62(1), 1–9,
764 doi:10.1111/j.1600-0870.2009.00421.x.

765 Parkinson, C. (2014), Spatially mapped reductions in the length of the Arctic sea ice
766 season, *Geophys. Res. Lett.*, 41(12), doi:10.1002/2014GL060434.

767 Polyakov, I. V., J. E. Walsh, and R. Kwok (2012), Recent Changes of Arctic Multiyear Sea
768 Ice Coverage and the Likely Causes, *Bull. Am. Meteorol. Soc.*, 93(2), 145–151,
769 doi:10.1175/BAMS-D-11-00070.1.

770 Reichle, R. H., R. D. Koster, G. J. M. De Lannoy, B. a. Forman, Q. Liu, S. P. P.
771 Mahanama, and A. Touré (2011), Assessment and Enhancement of MERRA Land
772 Surface Hydrology Estimates, *J. Clim.*, 24(24), 6322–6338, doi:10.1175/JCLI-D-10-
773 05033.1.

774 Rennermalm, A.K., L.C. Smith, J.C. Stroeve and V.W. Chu, (2009). Does sea ice
775 influenced Greenland ice sheet surface melt?, *Environ. Res. Lett.*, doi:10.1088/1748-
776 9326/4/2/024011.

777 Riener, M. M. et al. (2011), MERRA - NASA's Modern-Era Retrospective Analysis for



779 Research and Applications, *J. Clim.*, 24, 3624–3648, doi:10.1175/JCLI-D-11-00015.1.
780 Rinke, A., W. Maslowski, K. Dethloff, and J. Clement (2006), Influence of sea ice on the
781 atmosphere: A study with an Arctic atmospheric regional climate model, *J. Geophys.*
782 *Res.*, 111(D16), D16103, doi:10.1029/2005JD006957.
783 Screen, J.A. and I. Simmonds (2010), The central role of diminishing sea ice in recent
784 Arctic temperature amplification, *Nature*, 464, 1334–1337, doi:10.1038/nature09051.
785 Serreze, M.C., J. Stroeve, A.P. Barrett and L.N. Boisvert (2016), Summer atmospheric
786 circulation anomalies over the Arctic Ocean and their influences on September sea ice
787 extent: A cautionary tale, *J. Geophys. Res. Atmos.*, doi:10.1002/2016JD025161.
788 Serreze, M. C., A. P. Barrett, and J. J. Cassano (2011), Circulation and surface controls on
789 the lower tropospheric air temperature field of the Arctic, *J. Geophys. Res.*, 116,
790 D07104, doi:10.1029/2010JD015127
791 Serreze, M.C., A.P. Barrett, J.C. Stroeve, D.N. Kindig and M.M. Holland (2009), The
792 emergence of surface-absed Arctic amplification, *The Cryosphere*, 3, 11–19,
793 doi:10.5194/tc-3-11.2009.
794 Serreze, M.C., M.M. Holland, and J. Stroeve, (2007), Perspectives on the Arctic's
795 Shrinking Sea Ice Cover, *Science*, 16, 1533–1536.
796 Stroeve, J.C., A.D. Crawford and S. Stammerjohn (2016), Using timing of ice retreat to
797 predict timing of fall freeze-up in the Arctic, *Geophys. Res. Lett.*,
798 doi:10.1002/2016GL069314.
799 Stroeve, J.C., T. Markus, L. Boisvert, J. Miller and A. Barrett (2014), Changes in Arctic
800 Melt Season and Implications for Sea Ice Loss. *Geophysical Research Letters*,
801 doi:10.1002/2013GL058951.
802 Stroeve, J.C., M.C. Serreze, J.E. Kay, M.M. Holland, W.N. Meier and A.P. Barrett, (2012).
803 The Arctic's rapidly shrinking sea ice cover: A research synthesis, *Clim. Change*, doi:
804 10.1007/s10584-011-0101-1.
805 Stroeve, J. C., M. C. Serreze, A. Barrett, and D. N. Kindig (2011), Attribution of recent
806 changes in autumn cyclone associated precipitation in the Arctic, *Tellus A*, 63(4), 653–
807 663, doi:10.1111/j.1600-0870.2011.00515.x.
808 Stroeve, J., A. Frei, J. McCreight, and D. Ghatak. 2008. Arctic sea-ice variability revisited.
809 *Ann. Glaciol.*, 48(1): 71–81, doi:10.3189/172756408784700699.
810 Tedesco, M., X. Fettweis, P. M. Alexander (2015), MAR v3.2 regional climate model data
811 for Greenland (1958–2013). UCAR/NCAR - CISL - ACADIS.
812 Dataset. <http://dx.doi.org/10.5065/D6JH3J7Z>.
813 Tedesco, M., X. Fettweis, T. Mote, J. Wahr, P. Alexander, J.E. Box, and B. Wouters,
814 (2013), Evidence and analysis of 2012 Greenland records from spaceborne observations,
815 a regional climate model and reanalysis data, *The Cryosphere*, 7, 615–630.
816 Tedesco, M. and X. Fettweis (2012), 21st century projections of surface mass balance
817 changes for major drainage systems of the Greenland ice sheet, *Env. Res. Lett.*, 7,
818 045405.
819 Tedesco, M., X. Fettweis, M. R. van den Broeke, R. S. W. van de Wal, C. J. P. P. Smeets,
820 W. J. van de Berg, M. C. Serreze, and J. E. Box (2011), The role of albedo and
821 accumulation in the 2010 melting record in Greenland, *Environ. Res. Lett.*, 6(1),
822 014005, doi:10.1088/1748-9326/6/1/014005.
823 Tedesco, M. (2007), Snowmelt detection over the Greenland ice sheet from SSM/I
824 brightness temperature daily variations, *Geophys. Res. Lett.*, 34, L02504,
825 doi:10.1029/2006GL028466.
826 Tedesco, M., M. Serreze, and X. Fettweis (2008), Diagnosing the extreme surface melt



827 event over southwestern Greenland in 2007. *Cryos. Disc.* 2(3): 383–397.
828 van den Broeke, M., J. Bamber, J. Ettena, E. Rignot, E. Schrama, W.-J. van de Berg, E. van
829 Meijgaard, I. Velicogna and B. Wouters (2009), Partitioning recent Greenland mass
830 loss, *Science*, 326, doi:10.1126/science.1178176.
831 van den Broeke, M., and H. Gallée (1996), Observation and simulation of barrier winds at
832 the western margin of the Greenland ice sheet, *Q.J.R. Meteorol. Soc.*, 122, 1365–1383.
833 van Tricht, K., and Coauthors, (2016), Clouds enhance Greenland ice sheet meltwater
834 runoff, *Nat. Commun.*, 7, 10266, doi:10.1038/ncomms10266.
835 <http://www.nature.com/doifinder/10.1038/ncomms10266>.
836 Wang, J., J. Zhang, E. Watanabe, M. Ikeda, K. Mizobata, J.E. Walsh, X. Bai, and B. Wu
837 (2009), Is the dipole anomaly a major driver to record lows in Arctic summer sea ice
838 extent?, *Geophys. Res. Lett.*, 36, L05706, doi: 10.1029/2008GL036706.
839 Yulaeva, E., N. Schneider, D.W. Pierce, and T.M. Barnett (2001), Modeling of North
840 Pacific Climate Variability Forced by Oceanic Heat Flux Anomalies, *J. Clim.*, 14, 4027–
841 4046, doi: 10.1175/1520-0442(2001)014<4027:MONPCV>2.0.CO;2.
842 Zib, B. J., X. Dong, B. Xi, and A. Kennedy (2012), Evaluation and Intercomparison of
843 Cloud Fraction and Radiative Fluxes in Recent Reanalyses over the Arctic Using
844 BSRN Surface Observations, *J. Clim.*, 25(7), 2291–2305, doi:10.1175/JCLI-D-11-
845 00147.1.
846



847
848
849
850
851
852
853

Table 1. Climatological (1981-2010) mean values in length of open water season, together with climatological dates in early melt onset (EMO), continuous melt onset (MO), continuous freeze-up (FO) and melt season duration for 5 sea ice regions (excluding the North Atlantic where little sea ice exists). Corresponding mean dates in melt onset, freeze-up and duration are also shown for the Greenland drainage basins.

Region	Length of Open Water Season (days)	EMO (day of year)	MO (day of year)	FO (day of year)	Melt Duration (days)
<i>Sea Ice Regions</i>					
Baffin Bay	104	146	155	291	136
Davis Strait	220	133	143	321	188
North Atlantic	360	110	134	313	178
Greenland Sea	227	143	148	267	119
Lincoln Sea	0	162	172	232	60
<i>Greenland Ice Sheet Drainage Regions</i>					
Baffin Bay		162	164	232	68
Davis Strait		149	157	247	90
North Atlantic		143	145	234	89
Greenland Sea		163	166	231	65
Lincoln Sea		166	167	230	63

854
855



856
 857
 858
 859
 860
 861
 862

Table 2. Trends from 1979 to 2015 in length of open water season, together with trends in melt onset, freeze-up and melt season duration for 5 sea ice regions (excluding the North Atlantic where little sea ice exists). Corresponding trends in melt onset, freeze-up and duration are also shown for the Greenland drainage basins. Only values for the continuous melt onset and freeze-up periods are listed. Trends are given as days per decade. Statistical significance of trend at 95 and 99% are denoted by ⁺ and ⁺⁺, respectively.

Region	Open Water Trend (days/dec)	EMO Trend (days/dec)	MO Trend (days/dec)	FO Trend (days/dec)	Melt Duration Trend (days/dec)
<i>Sea Ice Regions</i>					
Baffin Bay	12.6 ⁺	-5.7 ⁺⁺	-8.3 ⁺⁺	7.8 ⁺⁺	16.1 ⁺⁺
Davis Strait	15.9 ⁺	-4.7 ⁺	-6.7 ⁺⁺	5.0 ⁺⁺	11.7 ⁺⁺
North Atlantic	N/A	-6.9 ⁺⁺	-7.3 ⁺⁺	8.9 ⁺⁺	16.3 ⁺⁺
Greenland Sea	15.2 ⁺	-6.7 ⁺⁺	-3.8 ⁺	2.1	5.9 ⁺
Lincoln Sea	-0.1	-4.0 ⁺⁺	-3.9 ⁺⁺	1.6	5.5 ⁺⁺
<i>Greenland Ice Sheet Drainage Regions</i>					
Baffin Bay		-6.1 ⁺⁺	-6.4 ⁺⁺	4.6 ⁺	11.1 ⁺⁺
Davis Strait		-6.3 ⁺⁺	-10.5 ⁺⁺	8.2 ⁺⁺	18.7 ⁺⁺
North Atlantic		-10.7 ⁺⁺	-16.4 ⁺⁺	5.7 ⁺⁺	22.1 ⁺⁺
Greenland Sea		-6.1 ⁺⁺	-6.8 ⁺⁺	7.6 ⁺⁺	14.4 ⁺⁺
Lincoln Sea		-5.1 ⁺⁺	-5.9 ⁺⁺	6.8 ⁺⁺	12.7 ⁺⁺

863
 864



865
866
867
868

Table 3. Percentage of grid cells with a significant correlation at $\alpha = 0.05$ relative to the total grid cells of the unmasked ice sheet. The correlation is between ice sheet meltwater production and area-averaged sea ice concentration anomalies in the Beaufort Sea and Baffin Bay (hatched regions in Figures 5a and 6a, respectively).

Month	Beaufort Sea		Baffin Bay	
	Simple Correlation (%)	Partial Correlation (%)	Simple Correlation (%)	Partial Correlation (%)
June	87.0	81.0	17.3	20.2
July	31.2	13.4	11.1	2.1
August	32.6	12.5	12.5	9.4

869
870
871



872
 873

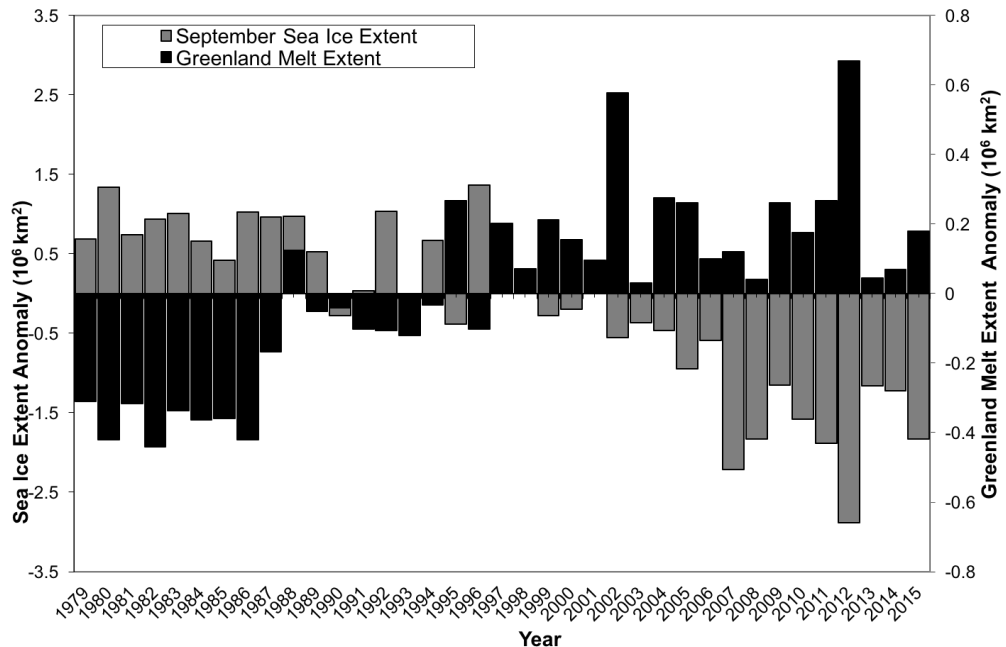
Table 4. Summary table of results discussed in the main body of the manuscript

Analysis Performed	Davis Strait	Baffin Bay	Lincoln Sea	Greenland Sea	North Atlantic
SVD: GrIS \leftrightarrow SIC (Fig. 3)		June			
SIC trends (Fig. 4)	Reduced in all seasons	Reduced in all seasons	No change	Positive near the coast in spring and winter	N/A
Open water days (Fig. 4)	Increase	Increase	Increase	Increase	Increase
OWF trends (Fig. 5)	Positive throughout shoulder seasons	Sharp peak in June and October	mixed	Positive throughout year, no sharp peaks	N/A
Relative start of melt on SIC and GrIS (Table 2)	SIC MO earlier, SIC FO later	SIC MO earlier, SIC FO later	SIC and GrIS similar	SIC MO earlier, SIC FO later	N/A
Trends in timing of EMO, MO, FO (Table 2, Fig. 6)	MO earlier FO later	MO earlier FO later	MO earlier FO later	MO earlier FO later	N/A
Synchronicity between GrIS and SIC EMO, MO, FO time series		R > 0.6 for MO, FO R > 0.5 for detrended data	R > 0.6 for MO, FO R > 0.5 for detrended data	R > 0.5 for EMO	
Latent heat fluxes (Fig. 7)	positive all year	positive all year	positive in summer	positive all year	N/A
Sensible heat fluxes (Fig. 7)	Positive spring/fall	Positive JASO	Negative all year	Positive spring/fall	N/A
Early/late MO years composites (Fig. 7)	Positive in winter, negative rest of year	Majority of positive anomalies	mixed	mixed	
Net longwave fluxes (Fig. 8)	Positive anomalies in spring	Positive anomalies in spring	Positive anomalies in spring	Positive anomalies in spring	N/A

874
 875
 876
 877



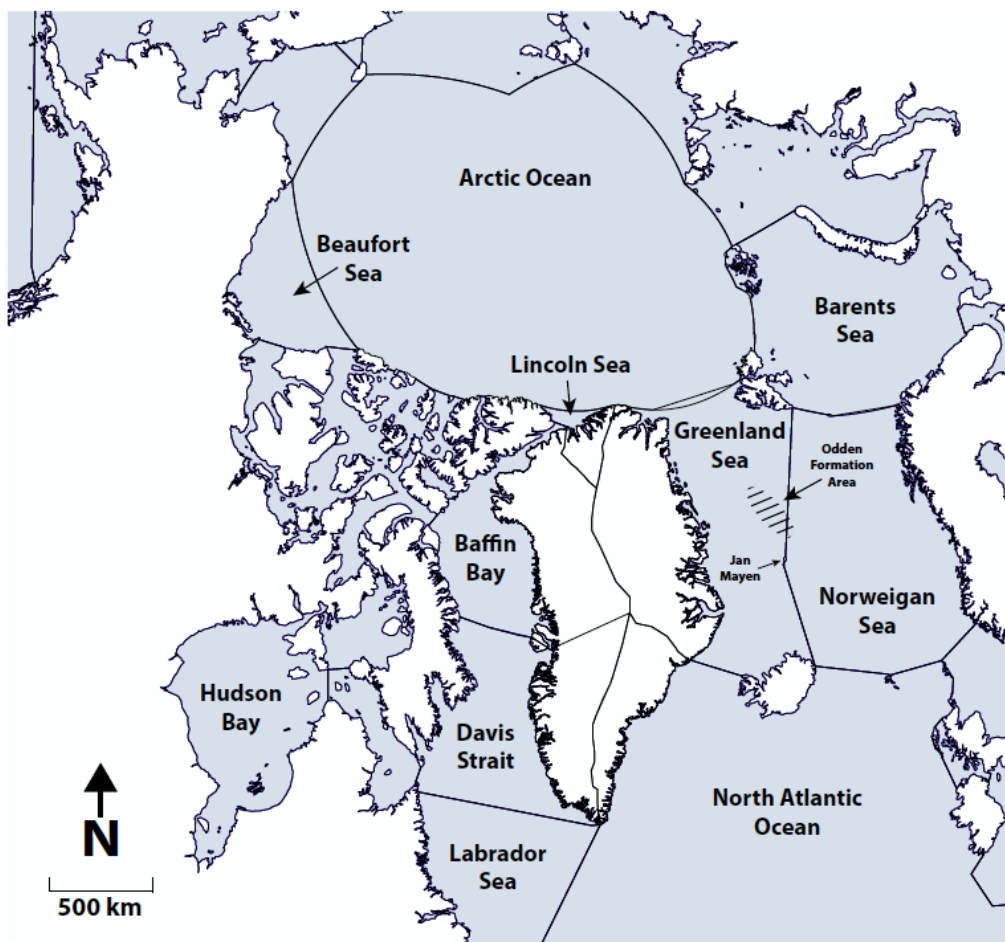
878



879
880 **Figure 1.** Time-series of September sea ice extent and Greenland surface melt extent
881 anomalies from 1979 to 2015.
882

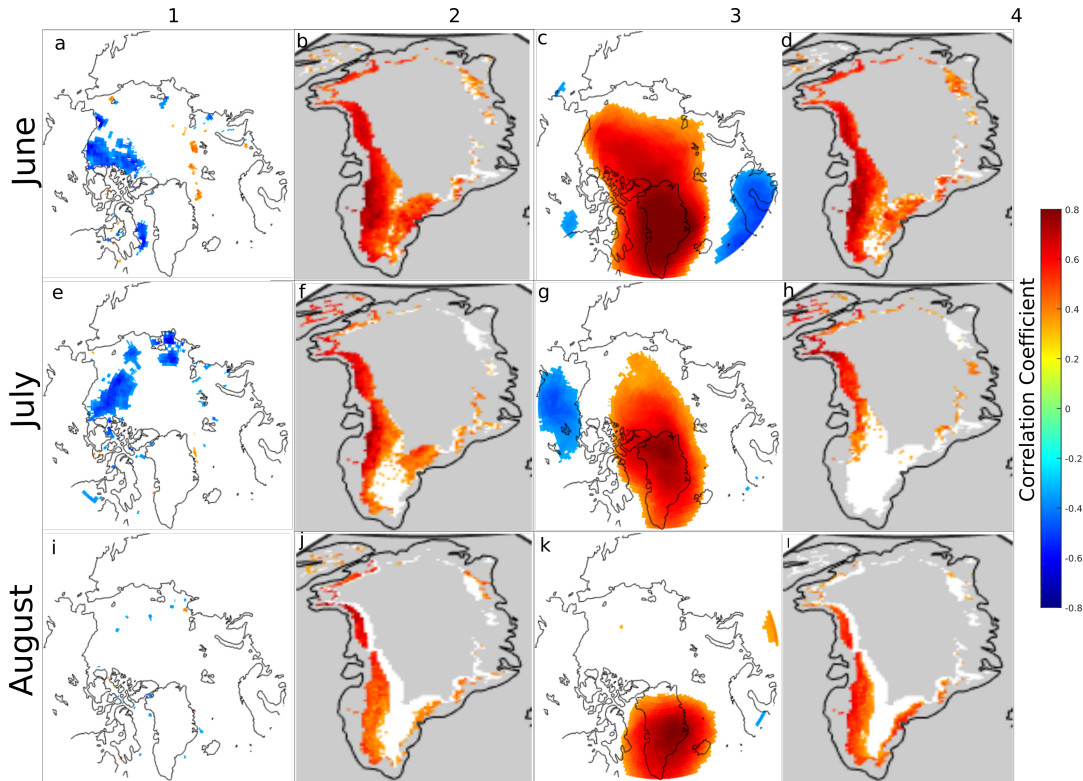


883



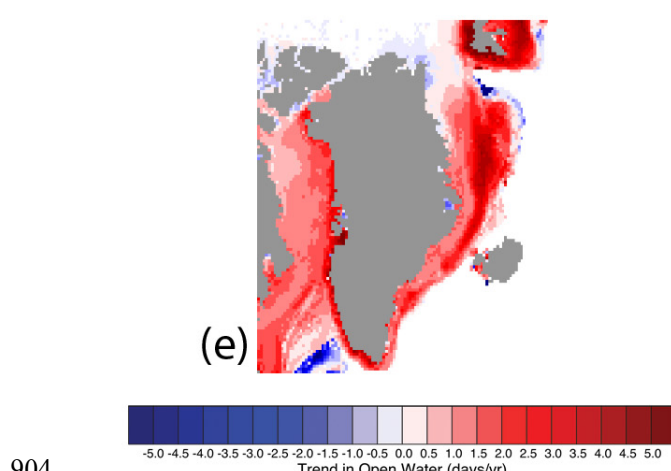
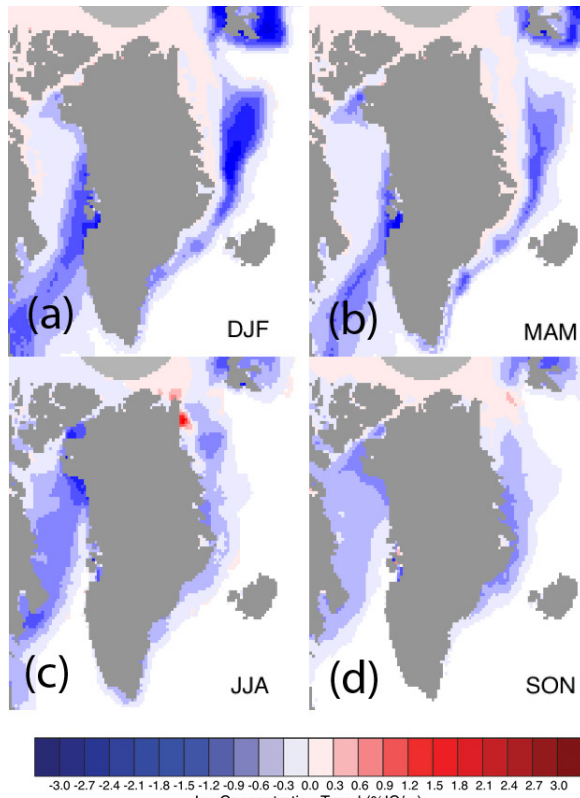
884
885
886
887
888
889
890
891
892

Figure 2. Map of study area, including the six sea ice and Greenland drainage sectors used in this study. The ice sheet regions are named after their adjacent sea (i.e. Davis Strait, Baffin Bay, Lincoln Sea, Greenland Sea, and the North Atlantic). The approximate area where the Odden sea ice featured used to formed is indicated with hatched lines. The ocean boundaries are defined by the International Hydrographic Organization (VLIZ (2005). IHO Sea Areas. Available online at <http://www.marineregions.org/>.)



893
894
895
896
897
898
899
900
901
902
903

Figure 3. Heterogeneous correlation between variables in the leading SVD mode in JJA. Column 1 is the correlation between sea ice concentration and EC_{GrIS} . Column 2 is the correlation between meltwater production and EC_{SIC} . Column 3 is the correlation between 500 hPa geopotential heights and EC_{GrIS} . Column 4 is the correlation between meltwater production and the EC_{500} . Correlation coefficients are not considered over the masked gray regions, and only correlations significant at $\alpha = 0.05$ are shown. All data are anomalies relative to 1979-2015 means with the least-squares trend line removed.

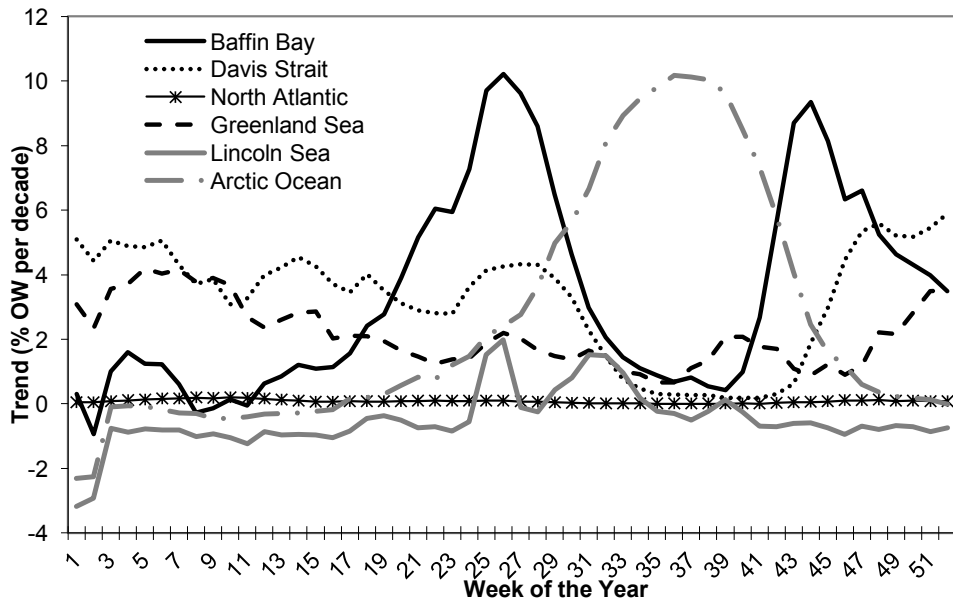


904
905
906
907
908
909
910

Figure 4. Seasonal trends in sea ice concentration from 1979 to 2015 (a-d) and number of ice free days (e).



911



912

913

914

915

916

Figure 5. Trends in regional open water fraction (OWF) surrounding the Greenland Ice Sheet, computed from 1979 to 2014.

917

918

919

920



921
922

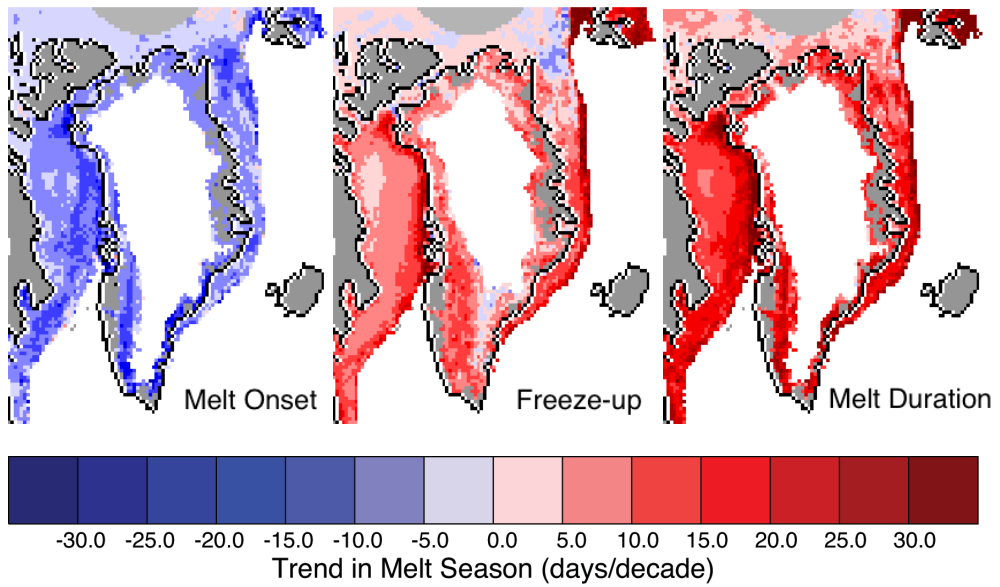
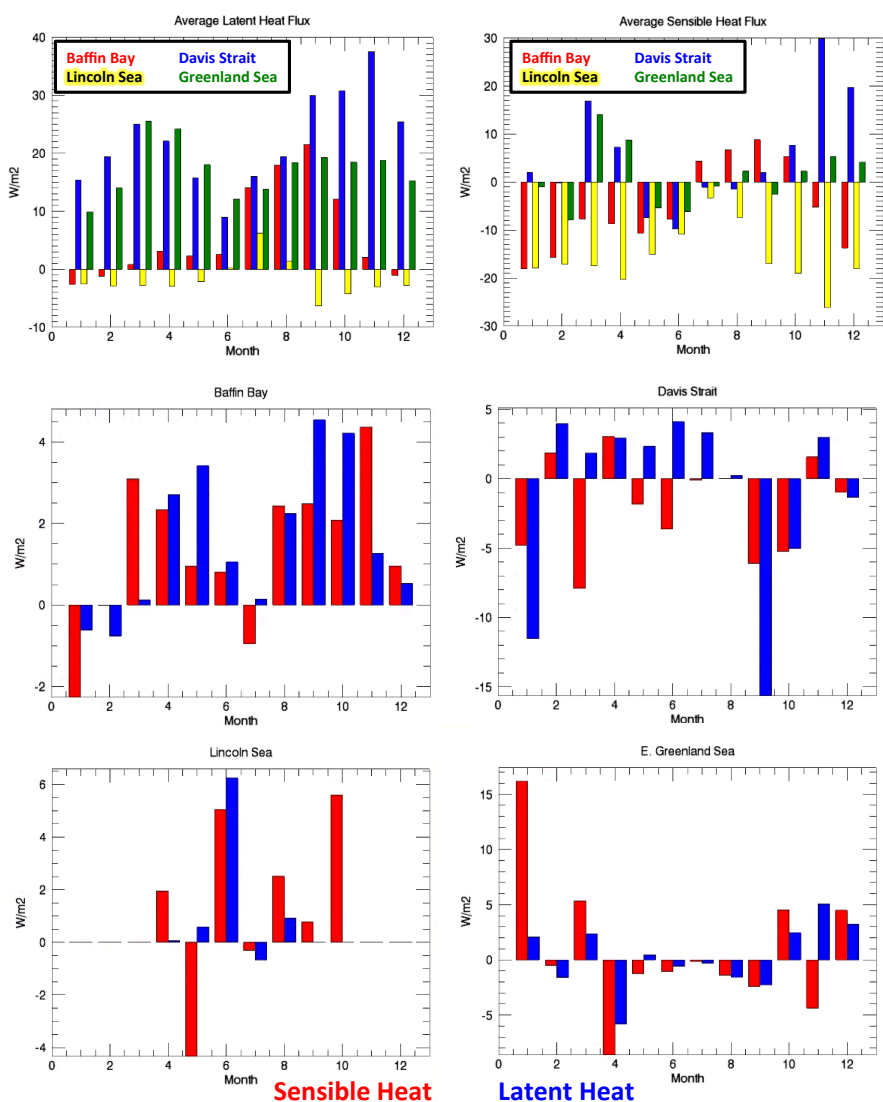


Figure 6. Trends in melt onset (top), freeze-up (middle) and total melt season length (bottom) for sea ice and Greenland from 1979 to 2015.



928

929

930

931 **Figure 7.** Top row graphs show the 2002 to 2015 average latent and sensible heat
 932 fluxes for each ocean region (denoted by color). The sign convention is such that
 933 positive fluxes are directed from the ocean to the atmosphere. Bottom two row

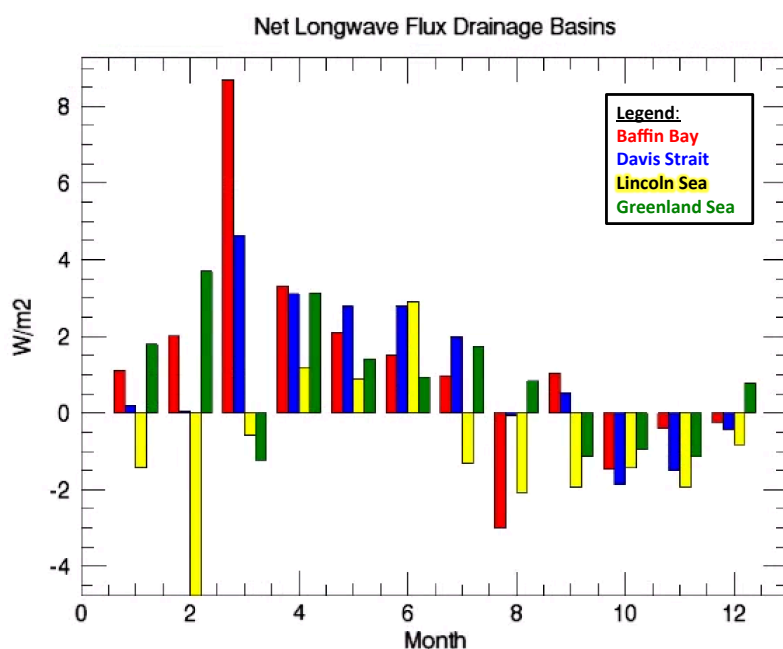


934 graphs show the early minus late melt onset years for each region of the positive (into
935 the atmosphere) sensible (red) and latent (blue) heat fluxes.

936

937

938



939

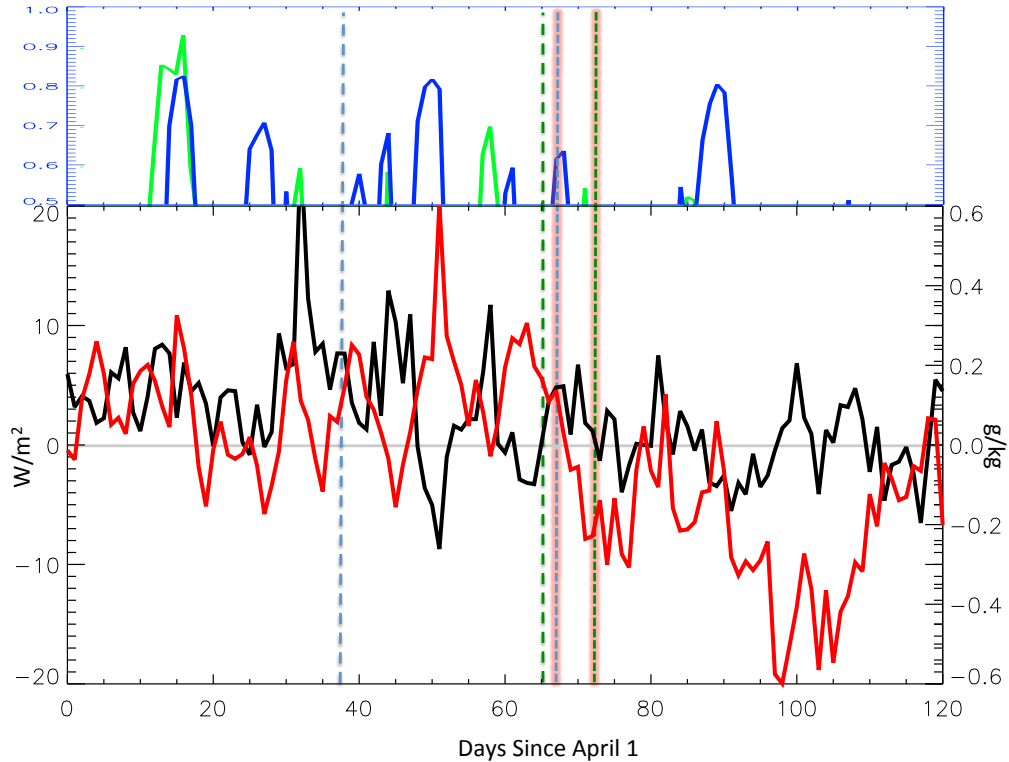
940

941 **Figure 8.** Net longwave flux (downwelling longwave flux – upwelling longwave flux)
942 for early MO minus late MO years for the drainage basins of the Greenland Ice Sheet,
943 where red bars are for Baffin Bay, blue bars are for Davis Strait, yellow bars are for
944 Lincoln Sea and green bars and for Greenland sea.

945

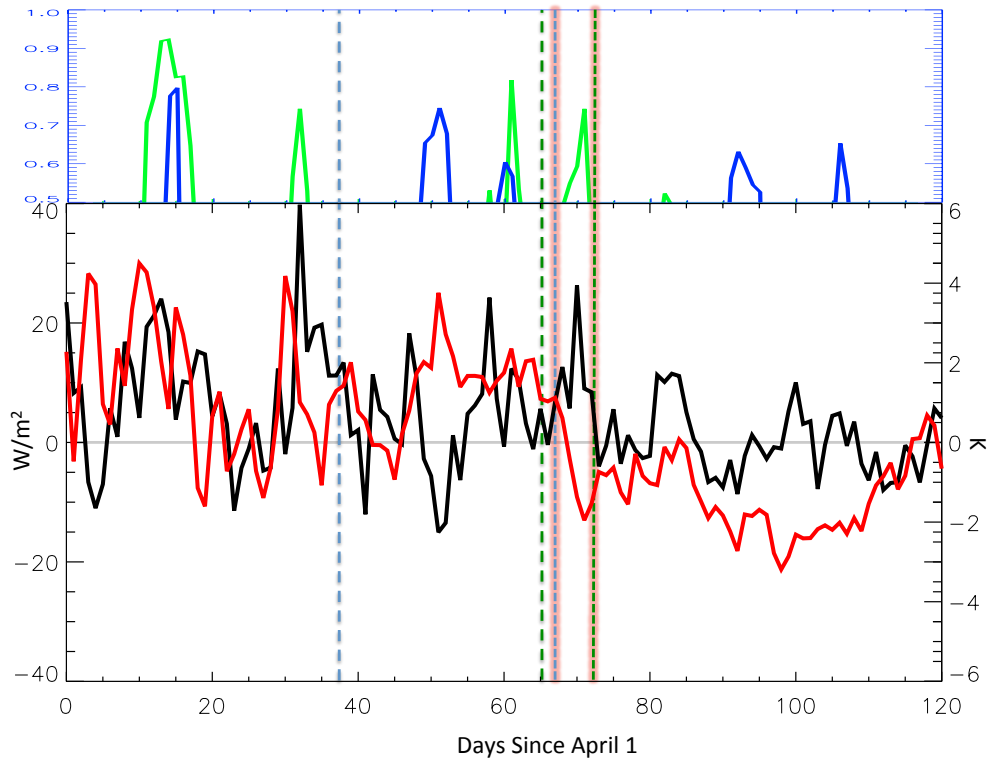


946
947
948



949
950
951
952
953
954
955
956
957
958
959
960

Figure 9a. Baffin Bay SIC region latent heat flux from early minus late MO years (black line) and Baffin Bay GrIS region specific humidity from early minus late MO years (red line). Dotted vertical lines represent the average early melt onset date for Baffin Bay (dotted blue), and average late melt onset date for Baffin Bay (dotted blue, red highlight), average early melt onset date for GrIS (dotted green), and average late melt onset date for GrIS (dotted green, orange highlight). The top portion of this figure shows the week lag-1 week lagged running correlations (between 0.5 and 1.0) for early melt years latent heat flux from Baffin Bay and specific humidity from GrIS (blue) and late melt onset latent heat flux from Baffin Bay and specific humidity from GrIS years (green).

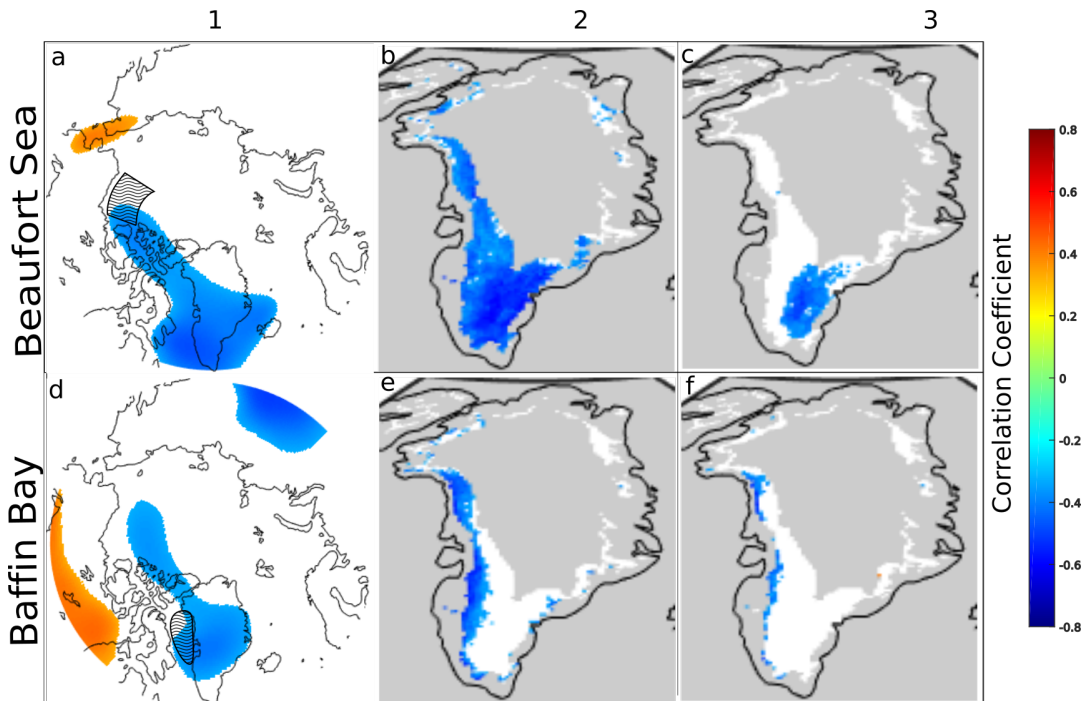


961
962
963
964
965
966
967
968
969
970
971
972
973

Figure 9b. Baffin Bay SIC region sensible heat flux from early minus late MO years (black line) and Baffin Bay GrIS region air temperature from early minus late MO years (red line). Dotted vertical lines represent the average early melt onset date for Baffin Bay (dotted blue), and average late melt onset date for Baffin Bay (dotted green), average early melt onset date for GrIS (dotted blue, red highlight), and average late melt onset date for GrIS (dotted green, orange highlight). The top portion of this figure shows the week lag-1 week lagged running correlations (between 0.5 and 1.0) for early years sensible heat flux from Baffin Bay and air temperature from GrIS (blue) and late melt onset sensible heat flux from Baffin Bay and air temperature from GrIS years (green).



974
975
976
977
978



979 **Figure 10.** June correlation between spatially averaged SIC in the hatched region and:
980 Column 1) 500 hPa geopotential height field, Column 2) Greenland meltwater
981 production, and Column 3) same as Column 2 but with the effect of the Greenland
982 Blocking Index removed (partial correlation). Correlation coefficients are not
983 considered over the masked gray regions. All data are anomalies relative to 1979-
984 2015 means with the least-squares trend line removed.
985
986

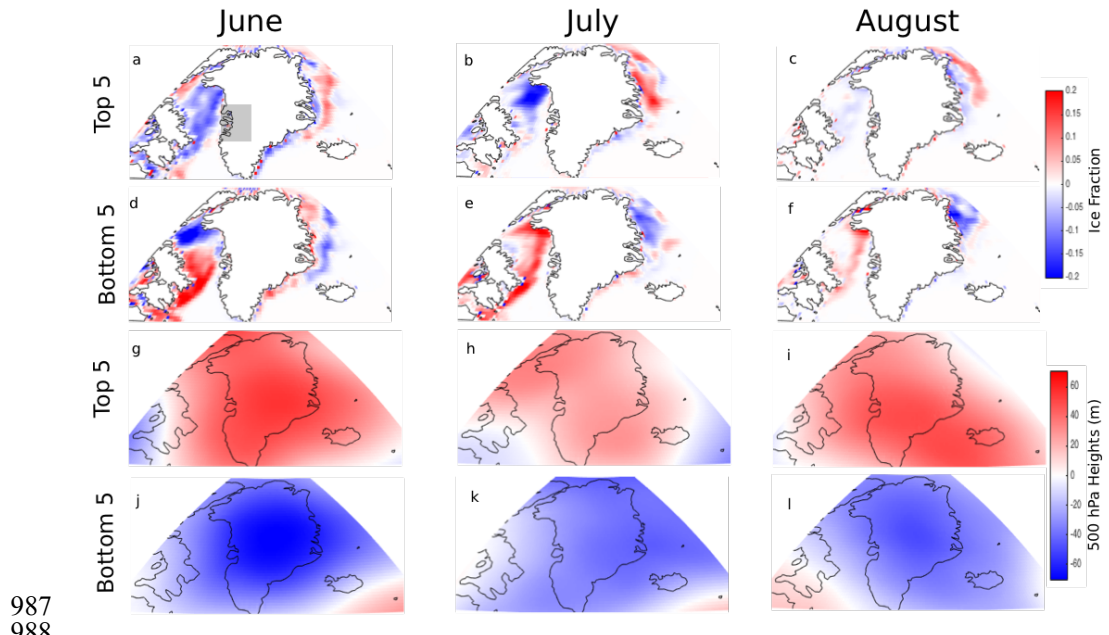
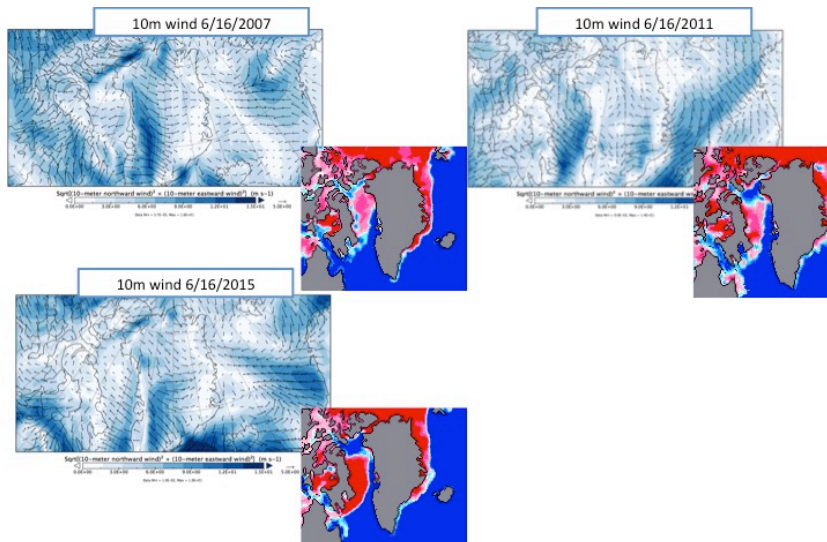


Figure 11. De-trended anomalies of SIC (a-f) and 500 hPa geopotential heights (g-l) averaged over the 5 highest and lowest melt years in June, July, and August as indicated by de-trended meltwater production anomalies in the indicated gray region of the ice sheet. Units are ice fraction (a-f) and m (g-l).

987
988
989
990
991
992
993
994
995

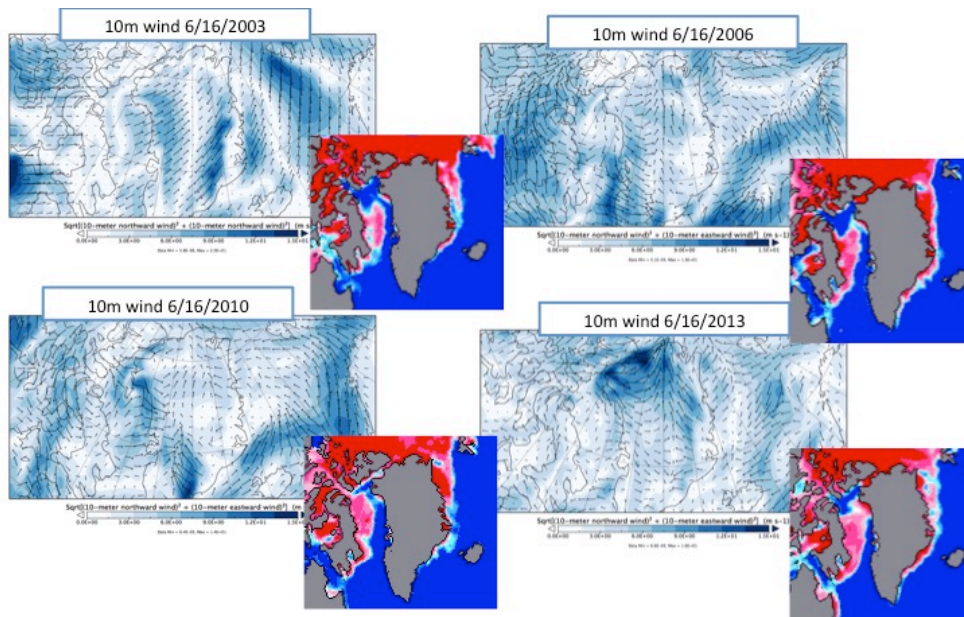


996



Late Melt Years

997



998
 999
 1000
 1001

Figure 12. Daily wind vectors at 10 meters from AIRS during 3 early sea melt years over Baffin Bay (top panel) and 4 late sea melt years (bottom) panel.